CYP3A4 inhibition and induction studies coupled to parallel artificial membrane permeability assay (PAMPA) for improved prediction of *in-vitro* botanical-drug interactions

by

Yilue Zhang

A thesis submitted to the Graduate Faculty of
Auburn University
in partial fulfillment of the
requirements for the Degree of
Master of Science

Auburn, Alabama
August 3, 2019

Keywords: *Euterpe oleracea* Mart.; Açaí; *Lepidium meyenii* Walpers; Maca; drug-botanical interaction; PAMPA

Approved by

Angela I. Calderón, Chair, Associate Professor of Drug Discovery and Development
Randall Clark, Professor of Drug Discovery and Development
Jack DeRuiter, Professor of Drug Discovery and Development
Satyanarayana R. Pondugula, Associate Professor of Anatomy, Physiology and Pharmacology

Abstract

The consumption of botanical dietary supplements (BDS) is a common practice among the US population. However, the potential for botanical-drug interactions exists, and their mechanisms have not been thoroughly studied. CYP3A4 is an important enzyme that contributes to the metabolism of about 60% of clinically used drugs. This study investigates the potential for CY3A4-mediated botanical-drug interactions of *Lepidium meyenii* Walpers (maca) root and *Euterpe oleracea* Mart. (açaí) berries since they are commonly used BDS that may be co-administered with CYP3A4-metabolized drugs. In an attempt to decrease the general discrepancy between in vivo and in vitro studies, the absorption profiles, particularly for passive diffusion, and metabolism profiles of plant extracts were investigated. Specifically, the parallel artificial membrane permeability assay (PAMPA) model was utilized to simulate intestinal filtration of passively diffused constituents of açaí and maca extracts. These were subsequently screened for in vitro liver CYP3A4 inhibition and induction. In the inhibition assay, midazolam was used as the probe substrate on genotyped human liver microsomes (CYP3A5 null), and the production of its 1′-substituted metabolite when co-cultured with extract treatments was monitored. In the induction assay, extract treatments were applied to human primary hepatocytes, and quantitative PCR analysis was performed to determine CYP3A4 mRNA expression. Moreover, an *in-vitro* LC-MS-based methodology was established to access human liver metabolites mediated by UGT or CYP enzymes. As a result, passively diffused constituents of the methanol açaí extract (IC_{50} of 28.03 µg/µL) demonstrated the highest inhibition potential, and, at 1.5 µg/µL, induced significant

changes in CYP3A4 gene expression. The composition of this extract was further investigated using the chemometric tool Mass Profiler Professional (MPP) on liquid chromatography-mass spectroscopy (LC-MS) data. Subsequently, five compounds of interest characterized by high abundance or high permeability were extracted for further study. This included efforts in effective passive permeability determination and structural elucidation by tandem mass spectrometry (MS/MS). Furthermore, a total of 9 metabolites of compounds in methanol açaí extract were separated and annotated.

Acknowledgements

First of all, I want to express my deepest appreciation to my advisor, Dr. Angela Calderón, for all the courage, help and guidance she gave to me. She was the one who offer me an opportunity to continue a career in pharmaceutical science when I hit the rock bottom. During the years in my Master's degree, she was always willing to share her ideas and experience, and I could always feel her concern and expectation to me. This thesis would not have been possible without her guidance.

I would like to thank the rest of my thesis committee members. I am more than thankful to Dr. Randall Clark who helped me to find where my interest lies by impressing me with his passion about the "puzzles" of mass spectrometry. As an expert in mass spectrometry, he inspired me a lot during my research. I am also grateful to Dr. Jack DeRuiter, my first teacher in the field of pharmaceutical science, for those fantastic lectures and those helpful advices. I want to take this opportunity to thank Dr. Satyanarayana R. Pondugula for his patience in training me in the research skills and his crucial input in my thesis.

In addition, I am grateful to my lab mates for their generous support. I want to thank Da Jung for teaching me the lab techniques when I first come to the lab, and for giving me the guidance about study and life. I want to express my gratitude to my other lab mates including Elizabeth Lopez, Turner Shirley, Tyler Wietlake, Madison Patrick and Hannah Kim for the valuable help they offered and the joy they brought. I also want to thank Chuan Wang, Mansour Alturki and Qianman Peng for their sincere concern.

I extend my sincere thanks to the amazing researchers I have collaborated with, including Dr. Douglas Goodwin and Hui Xu from the KatG project, and Dr. Mark Liles and Megan Sandoval-Powers from the microbial metagenomics project. I would like to thank Dr. Dejan Nikolic from the University of Illinois at Chicago for providing insightful comments on my spectra interpretation. I also want to thank Agilent engineers and application chemist on LC-MS, especially Dr. Julie Hagel from Agilent Technologies, for their continuous help in my research.

I want to thank all the non-academic staff, especially Jennifer Johnston, Kaleia Williams and Christopher Smith, for always being around to help.

I am indebted to the Auburn University Research Initiative in Cancer (AURIC) for the financial support to my research.

Last but not least, I want to thank all my family and friends. Special thanks to my dearest friend Minsi Li from the University of Western Ontario, who stands by me through the best and the worst of times. Special thanks to my dearest friends Luoqi Miao, Pengmin Pan and Jipeng Qian, for making my life in Auburn so colorful and bright. Special thanks to my cousin, Chriscelle Cui, for her support and care. Special thanks to my uncle and my career mentor, Yuan Song, for directing me the way to my dream. Special thanks to my dearest parents, Fan Wang and Shangda Zhang, for making me surrounded by love every single day.

Table of Contents

List of Figures

List of Tables

List of Abbreviations

ADME absorption, distribution, metabolism, and excretion

ACN acetonitrile

AEs adverse events

ANOVA analysis of variance

BDS botanical dietary supplements

CAM complementary and alternative medicine

CYP cytochrome P450

DMSO dimethyl sulfoxide

DSLD Dietary Supplement Label Database

ESI positive electrospray ion

FAERS Food and Drug Administration Adverse Event Reporting System

FDA U.S. Food and Drug Administration

GST glutathione S-transferase

HLM human liver microsomes

IS internal standard

LC-MS liquid chromatography-mass spectroscopy

LOD limit of detection

LOQ limit of quantification

MPP Mass Profiler Professional

MS/MS tandem mass spectrometry

NAT N-acetyltransferase

NMR nuclear magnetic resonance

PAMPA parallel artificial membrane permeability assay

Pe effective passive permeability

P-gp P-glycoprotein

RIF rifampicin

SULT sulfotransferase

UGT UDP-glucuronosyltransferase

UV-VIS ultra-violet visible spectroscopy

Chapter 1: Introduction

1.1 Botanical-drug interactions

1.1.1 Use of botanical dietary supplement among U.S. cancer patients

As defined by Dietary Supplement Health And Education Act of 1994, the term "dietary supplement (DS)" means a product (other than tobacco) intended to supplement the diet that bears vitamins, minerals, amino acids, botanicals, and/or other dietary substances. Botanical dietary supplement (BDS) is one of the subsets of DS which contains herbs or other botanicals. They can be prepared and sold in many forms including powders, tablets, capsules, gummies, teas, tinctures, and essential oils (Shipkowski et al., 2018).

As reported by Clarke et.al, nonvitamin, nonmineral dietary supplements, including BDS, were consistently the most popular complementary health approach (17.7%~18.9%) among U.S. adults from 2002 to 2012 (Clarke et al., 2015). Moreover, according to a study on National Health and Nutrition Examination Survey data from 1999 to 2014, around 15.5%~23.6% of U.S. cancer patients use BDS in the prior 30 days, while a smaller frequency of 12.3%~18.0% in BDS consumption was reported among adults without cancer (Li et al., 2018). This especially high prevalence of BDS among cancer patients may result from intentions of general health enhancement, side effect prevention (Tascilar et al., 2006) and pain relief (Zareba, 2009).

1.1.2 Concomitant botanical dietary supplements consumption with anticancer drugs

Patients usually self-administer complementary and alternative medicine, including BDS, in combination with conventional chemotherapeutics, and 20% to 77% of them do not disclose this to their physicians (Davis et al., 2012). Therefore, BDS consumption is an unknown variable when physicians administer prescription medications. In addition, adverse events (AEs) reporting patterns of concomitant BDS and anticancer drug use from the 2004–2015 U.S. Food and Drug Administration Adverse Event Reporting System (FAERS) database identified potential protective and risk signals with concomitant use of seven BDS and anticancer drugs (Fahim et al., 2018). Açaí was the only BDS that showed a potential increase reporting signal for serious AEs with anticancer drugs, while protective signals were noticed when CYP3A4-interactive drugs were taken with cranberry (*Vaccinium macrocarpon* Ait.), garlic (*Allium sativum* L.) and ginger (*Zingiber officinale* Rosc.) (Fahim et al., 2018).

In the worst-case scenario, drug pharmacokinetics can be significantly altered due to the co-administration of BDS and chemotherapeutic agents, leading to clinically unacceptable toxicities or decreased therapeutic effects. Notably, with the narrow therapeutic window of most anticancer agents, botanical-drug pharmacokinetic interactions are potentially dangerous (Awortwe et al., 2018; Scripture and Figg, 2006; Tascilar et al., 2006).

1.1.3 Botanical-drug pharmacokinetic interactions

Pharmaceutical agents undergo absorption, distribution, metabolism, and excretion (ADME) in the host after administration. Specifically, drugs can be metabolized through Phase I (oxidation, reduction, and hydrolysis) and/or Phase II (conjugation) reactions. The most important oxidative Phase I enzymes are cytochrome P450 (CYP) superfamily, where six isoforms (CYP1A2,

CYP2C9, CYP2C19, CYP2D6, CYP3A4 and CYP3A5) are responsible for the metabolism of 90% drugs (Lynch and Price, 2007). Phase II enzymes include uridine 5'-diphospho-glucuronosyltransferase (UDP-glucuronosyltransferase, UGT), sulfotransferase (SULT), glutathione S-transferase (GST), N-acetyltransferase (NAT), and methyltransferase. Through Phase I and Phase II reactions, the hydrophilicity or activity of drugs can be altered, thus facilitating their elimination in liver or kidney.

Botanical-drug pharmacokinetic interactions result from the pharmacokinetics alteration when a drug's ADME profile is interfered by the concurrent consumption of BDS. In a recent review paper, Sprouse et. al classified botanical-drug interactions as the inhibition or induction of (1) CYP and other phase I enzymes; (2) UGT and phase II enzymes; (3) drug transporters and drug-efflux proteins (Sprouse and van Breemen, 2016). For example, St. John's wort (*Hypericum perforatum* L.) has the potential to induce the expression of both P-glycoprotein (P-gp) transporters and several CYP enzymes, including CYP3A4, CYP2E1 and CYP2C19 (Izzo, 2012). Therefore, it could influence the pharmacokinetics of drugs which are the substrates of P-gp and/or CYPs.

1.1.4 CYP3A4-mediated botanical-drug interaction

As the main Phase I metabolizing enzyme, CYP3A4 is a key CYP isoform and responsible for biotransformation of approximately 60% of clinically used drugs, including most cancer chemotherapeutics (Scripture and Figg, 2006). It is mainly expressed in the small intestine and liver of human adults (de Wildt et al., 1999). For CYP3A4-metabolized drugs, inhibition of CYP3A4 may lead to an increase in their systemic bioavailability, resulting in intolerable toxicity; while induction of CYP3A4 expression can cause a loss in bioavailability and decreased drug efficacy. On the other hand, the blood concentration of CYP3A4-activated prodrugs like

ifosphamide and trophosphamide (Ortiz de Montellano, 2013) would be influenced by CYP3A4 inhibitors or inducers in a reverse manner. Several BDS have been shown to inhibit or induce CYP3A4 to varying extents preclinically and clinically, including Echinacea (*Echinacea purpurea* (L.) Moench), Goldenseal (*Hydrastis canadensis* L.) and St. John's wort (Sprouse and van Breemen, 2016).

1.2 Reasons causing the discrepancy between *in-vivo* and *in-vitro* botanical-drug interaction studies

Preclinical research of hepatic botanical-drug interactions, including *in-vivo* and *in-vitro* studies, is often conducted prior to human studies. Commonly used *in-vitro* models include recombinant enzymes, human liver microsomes (HLM), human intestinal microsomes, S9 fractions, primary hepatocytes, and HepaRG cells (Markowitz and Zhu, 2012; Sprouse and van Breemen, 2016). However, supraphysiologic concentrations of plant constituents in these assays could lead to a discrepancy between preclinical and clinical interaction data (Gurley et al., 2018). The causes for misinterpretation of *in vivo* concentration of botanicals include using inappropriate solvent for dissolution and omission of absorption and metabolism profiles. Furthermore, the complexity of composition of phytochemicals adds another layer of challenge in prediction of botanical-drug interactions *in-vitro.*

1.2.1 Solvent selection

Solubility is the maximum amount of a chemical substance dissolved in a fixed amount of solvent to form a homogeneous mass. To reach the maximum solubility of botanicals, an organic solvent such as dimethyl sulfoxide (DMSO), is commonly added in *in-vitro* assay buffers. However, while

some of the compounds solubilize in the assay matrix, they may not be dissolved in gastrointestinal fluids inherently. Therefore, the potential of botanical-drug interactions can be overestimated by inducing those solubility-aiding agents into reaction matrix or culture media (Gurley et al., 2018; Markowitz and Zhu, 2012). In addition, inappropriate selection of solvent can lead to degradation of sensitive phytochemicals. For instance, anthocyanins are subject to degradation under higher pH and higher temperature, so buffers mimicking physiological conditions may generate more accurate predictions in dissolution compared to pure water (Loypimai et al., 2016).

It may be worth noting that according to the guidance of industry by U.S. Food and Drug Administration (FDA), a buffered aqueous medium with pH range 1.2 to 6.8 is recommended for dissolution testing of immediate release solid oral dosage forms. It is also stated in the guidance that an adjusted amount of surfactant (e.g. sodium lauryl sulfate) is recommended be added for poorly solubilized drugs (FDA, 2003). In order to mimic the GI fluids in *in-vitro* assays, similar experimental settings may be utilized for dissolution of botanicals.

1.2.2 Intestinal metabolism

Constituents of BDS may undergo extensive intestinal first-pass metabolism before reaching liver or site of actions. Moreover, phytochemicals can be metabolized to a much larger extent than conventional drugs whose active components are normally developed to be bioavailable or designed as prodrugs (Markowitz et al., 2008). Phytochemicals may be subject to enteric hydrolysis and phase II metabolism in intestinal epithelial cells, while gut microflora can also contribute to biotransformtion via hydrolysis and fermentation in colon (Lampe and Chang, 2007). Enzymes involved include brush border membrane-bound β-glucosidases, UGT and SULT in host.

In addition, gut bacterial β-glucosidases, CYP and other phase I enzymes that can metabolite phytochemicals are also responsible for intestinal metabolism (Lampe and Chang, 2007).

Intestinal metabolism can upregulate or downregulate the bioactivities of botanical components significantly, thus contributing to their potential to cause drug-botanical interactions. For instance, soy isoflavone daidzein is reported to have less biological activity than its intestinal metabolite, equol (Atkinson et al., 2005).

However, intestinal metabolism profiles are rarely considered in *in-vitro* studies, which can lead to misleading conclusion (Gurley et al., 2018). In a bioassay, it is a common practice to apply BDS extracts directly on cultured cell lines, cell fractions (*e.g.* microsomes) or other tested materials.

1.2.3 Absorption profiles

Orally administered drugs and dietary supplements can be absorbed through various mechanisms, including passive diffusion, carrier-mediated (active or facilitated) transport and pinocytosis. However, some constituents of BDS (e.g. many of polyphenols) are very poorly absorbed when consumed orally (Kidd, 2009). Therefore, the absorption profiles of botanicals should be considered to avoid overestimation of botanical-drug interactions in an *in-vitro* study.

Determination of the intestinal permeability properties (or absorption profiles) of drug candidates is a primary consideration in studies performed during lead selection and optimization (Balimane et al., 2006). This strategy can be effectively utilized in early stage prediction of the absorption profiles of BDS, and furthermore, it can be used in botanical-drug interactions.

Passive diffusion is the major absorption mechanism for medicines (Balimane et al., 2006). Parallel artificial membrane permeability assay (PAMPA) is a robust method to predict the transcellular passive absorption through the gastrointestinal tract. Furthermore, PAMPA has been

used to determine primary permeability of natural products during early bioavailability screening because of its high throughput capability and correlation with *in-vivo* absorption data (Awortwe et al., 2014; Petit et al., 2016).

Another common *in-vitro* model to predict likely gastrointestinal permeability of drug is Caco-2 cell line. It is originally derived from a colon carcinoma, and it shares a couple of identical characteristics with human small intestine, including expression of membrane efflux proteins (P-gp and MRP 1,2,3), CYP450 enzymes and phase II enzymes (Lea, 2015). Moreover, a good correlation exists between the predicted permeability of substances via Caco-2 model and human studies (Lea, 2015).

1.2.4 Liver metabolism

Similar to intestinal metabolism, hepatic metabolites of constituents in botanicals are sometimes responsible for drug-botanical interactions. For example, the liver metabolite of glabridin in *Glycyrrhiza glabra* were demonstrated to be an irreversible inhibitor of CYP3A4 after P450-mediated biotransformation (Huang et al., 2015). Therefore, liver metabolism should be considered to evaluate BDS in the overall potential causing drug-botanical interactions.

Also, phase II metabolism can alter the bioactivities of certain substances. For instance, clopidogrel could be converted to a strong CYP2C8 inhibitor of after glucuronidation (Tornio et al., 2014). However, according to an exhausted literature search, there was no evidence of bioactivity variation of herbal constituents after phase II transformation. Considering that the glucuronide and sulfate forms can be excreted rapidly (Kidd, 2009), phase II metabolism may not be one of the primary determinants in botanical-drug interactions predictions.

1.3 Project rationale

Euterpe oleracea Mart. (açaí) is a tropical palm tree originally from the Amazon belonging to the Arecaceae family and the genus *Euterpe* (Yamaguchi et al., 2015). Documented *in vitro* pharmacological screening assays of açaí berry extracts have reported antioxidant, anti-proliferative, cytoprotective and cancer-related anti-inflammatory activities (Chin et al., 2008; Rocha et al., 2007; Schauss et al., 2006). *Lepidium meyenii* Walpers (maca) is a cruciferous plant that belongs to the Brassicaceae family and *Lepidium* genus (Hermann, 1997; Quiroz et al., 1997). Most phytosterols extracted from maca (Dini et al., 1994; Zheng et al., 2000) reportedly exhibit anticancer, antioxidant and anti-inflammatory activities (Cui et al., 2005). Various claims of açaí's (Jensen et al., 2008; Mertens-Talcott et al., 2008; Sadowska-Krepa et al., 2015) and maca's (Nachshon-Kedmi et al., 2004; Sandoval et al., 2002) potential clinical benefit most likely contribute to the increased consumption of açaí and maca dietary supplements by cancer patients to complement their conventional chemotherapeutic medicines. Furthermore, adverse events (AEs) reporting patterns of concomitant BDS and anticancer drug use from the 2004–2015 U.S. Food and Drug Administration Adverse Event Reporting System (FAERS) database exhibited potential protective and risk signals with concomitant use of seven BDS and anticancer drugs, and açaí was the only BDS that showed a potential increase reporting signal for serious AEs with anticancer drugs (Fahim et al., 2018). Based on these findings, we examined the potential mechanism of botanical-drug interaction of açaí and maca. Specifically, the CYP3A4 inhibition and induction potentials of passively diffused compounds in maca and açaí extracts utilizing PAMPA were evaluated, and the chemical profiling of the most active extract was performed. We also elucidated the structures of compounds characterized by highest abundance and highest

permeability in the most active extract, followed by a Phase I and Phase II metabolism study of the targeted compound whose standard compound was commercially available.

1.4 Research objectives

The goal was to establish a reliable and clinically relevant strategy for evaluation of CYP3A4-mediated botanical-drug interactions using maca and açaí, as well as to develop a novel method for data processing in permeability studies.

Chapter 2: Development and optimization of methodologies for evaluating CYP3A4-mediated botanical-drug interaction

2.1 Materials and methods

2.1.1 Chemicals

Açaí berry powder (Lot #20569) and maca powder (Lot #21780) were supplied by Mountain Rose Herbs (Eugene, OR). The materials were analyzed, examined, and authenticated by Elan Sudberg and Sidney Sudberg from Alkemist Labs (Costa Mesa, CA, USA), and the authentication information was listed in Tables 1.1 and 1.2. Açaí dietary supplement standardized capsules (ADSC-1) were sourced from Nature's way (green bay, WI, lot #20047767), and açaí dietary supplement vegetarian capsules (ADSC-2) were sourced from NATROL (Chatsworth, CA, lot #2070593).

Table 1.1. Authentication information of açaí berry powder.

Title	Açaí Berry powder
Plant part	Fruit
Sample description	~78 g in a zip locked bag
Form of botanical	Crude plant powder
Appearance	Brown fine powder
Lot	20569
Sample	AAV16113MRH1_1
Latin name	*Euterpe oleracea*
Supplier	Mountain Rose Herbs

Reference sample	Lane 2 (3µl) (AAV7509MRH) (Fruit); Lane 3 (3µl) (AAV33808AÇAÍ) (Fruit); Lanes 6(4µl), 7(2µl) (AAV22609NOW) (Skin and pulp) *Euterpe oleracea*; authenticated by macroscopic, microscopic and/or TLC studies according to the reference source cited below, held at Alkemist Labs, Costa Mesa, CA
Reference source	Method developed by Alkemists Laboratories SOP-700-0001-R3
Analyst	JN, ML, RT 35724
Sample prep	Add 0.3 g sample into 3 mL CH_3OH. Sonicate and heat at 50 ˚C for 0.5 hrs.
Stationary phase	Silica gel 60, F254, 10 x 10 cm HPTLC plates
Mobile phase	Acetone: toluene: HCOOH [5/4/1]
Detection	(1) UV 365 nm (2) 10% Ethanolic H_2SO_4 115 ˚C 15 min UV 365 nm
Reference standard	Lanes 1 (3µl) and 8 (3µl) L-ascorbic acid (10930EE, Sigma-Aldrich, ~0.1% in CH_3OH
Comments and conclusions	Yellow line = sample origin @ 10 mm, red line = solvent front @ 70 mm. Lanes 4, 5 are test sample Açaí Berry Powder (20569). Lanes 2, 3, 6, 7 are the authenticated reference samples used for comparison. This test sample, Açaí Berry Powder (20569), is consistent with the chromatographic profile of the reference samples of *Euterpe oleracea*, 20 used above. This test sample, Açaí Berry Powder (20569) has characteristics of *Euterpe oleracea* fruit.
Note	The above conclusion may be a function of the natural variance found in botanicals. The growing and drying conditions, age, seasonal variations etc. all play a role in the phytochemical fingerprint of botanicals and variations are expected.

Examined, reviewed & authorized by	Elan Sudberg, CEO, Alkemist Labs
Work performed at	Alkemist Labs 1260 Logan Ave B2 Costa Mesa, CA 92626 714-754-4372 714-668-9972 (Fax) Email: sales@alkemist.com Web Site: www.alkemist.com
Report date	06/14/13

Table 1.2. Authentication information of maca powder.

Title	Maca powder
Plant part	Root
Sample description	Clear reclosable plastic bag
Form of botanical	Crude plant powder
Appearance	Sand-colored powder
Lot	21780
Sample	GC35614MRH1_1
Latin name	*Lepidium meyenii* Walp. [Brassicaceae]
Supplier	Mountain Rose Herbs
Reference sample	GC33208NI1; GC3803MP *Lepidium meyenii* Walp. [Brassicaceae] authenticated by macroscopic, microscopic &/or TLC studies held at Alkemist Labs, Costa Mesa, CA
Reference source	Internal reference sample SOP-1000-0001-R1 USP-PF, Vol. 27(2) (Mar.-Apr. 2001); Official methods of analysis of AOAC. 16th Ed.

Analyst	E. Sudberg
Magnification	400X
Chemical reagents	Acidified chloral hydrate glycerol solution
Sample findings	(1) oval and irregular starch granules (2) long narrow scalariform treachery vessels
Comments and conclusions	The sample is representative of *Lepidium meyenii* Walp. [Brassicaceae] root based on reference samples and the consistent characteristic cellular structure of a root. The characteristic cellular structures identified in this sample are the oval and irregular starch granules seen in monograph (2) and long narrow scalariform treachery vessels seen in monograph (3). The test sample, maca powder (21780), is consistent with the microscopic characteristics of the reference samples of *Lepidium meyenii* Walp. [Brassicaceae] used above & is characteristic of *Lepidium meyenii* Walp. [Brassicaceae] root.
Note	The presence of soluble excipients and other plant species material was not detected in this test sample.
Examined, reviewed & authorized by	Sidney Sudberg, Director, Alkemist Labs
Work performed at	Alkemist Labs 1260 Logan Ave B2 Costa Mesa, CA 92626 714-754-4372 714-668-9972 (Fax) Email: sales@alkemist.com Web Site: www.alkemist.com
Report date	01/12/15

All solvents used were HPLC or LC-MS grade and purchased from Thermo Fisher Scientific (Atlanta, GA). DMSO, LC-MS grade formic acid, KH_2PO_4, Na_2HPO_4, $MgCl_2$, EDTA, midazolam,

and NADPH were purchased from Sigma-Aldrich (Allentown, PA). 1′-hydroxymidazolam and the internal standard $^{13}C_3$-1′-hydroxymidazolam were bought from Cayman (Ann Arbor, MI) and Corning (Woburn, MA), respectively.

Pooled HLM (Catalog #HMMCPL) were sourced from Thermo Fischer Scientific (Atlanta, GA). Genotyped HLM (Item No. H3A5. NA) were obtained from XenoTech (Kansas City, KS). Cryopreserved human primary hepatocytes (Catalog #HUCPI), thawing medium (Catalog #MCHT50), plating medium (Catalog #MP100), and maintenance medium (Catalog #MM250) were purchased from Lonza (Walkersville, MD).

Protocatechuic acid methyl ester was purchased from Oakwood Chemical (Estill, SC, USA). Homoeriodictyol was purchased from Alkemist Labs (Garden Grove, CA, USA). Dihydrokaempferol was purchased from Carbosynth (San Diego, CA, USA). All plant standard compounds had a purity greater than 90%.

Acrodisc® One PSF syringe filter with GXF/wwPTFE membrane was a gift from Pall Corporation (Ref #SAP-4919).

2.1.2 Plant extract preparation

2.1.2.1 Extraction from plant powder

After defatting via dichloromethane, the generated residue from açaí and maca powder was further extracted with methanol three times by sonication. The methanol extracts were combined and centrifuged at 4000 rpm at 4 °C for 20 min. The produced supernatant was filtered through a 0.2 µm polytetrafluoroethylene membrane filter and dried under high vacuum (295 mbar) at 40 °C.

For the acidic methanol extracts, a similar procedure was followed. Plant material powder was extracted three times with 70:30 acidic methanol: water (acid methanol comprises 0.1% v/v

hydrochloric acid). After centrifugation and filtration, the acidic methanol soluble portions were dried under vacuum (300 mbar down to 72 mbar) at 40°C.

To ensure complete evaporation of the solvents, plant extracts were further dried by nitrogen evaporation and lyophilization. The yields were 7.55% (w/w, related to extract ratio of 13:1) for açaí methanol extract, 14.54% (w/w, related to extract ratio of 7:1) for açaí acidic methanol extract, 11.90% (w/w, related to extract ratio of 8:1) for maca methanol extract, and 25.96% (w/w, related to extract ratio of 4:1) for maca acidic methanol extract.

2.1.2.2 Extraction from capsules

This experiment was performed on two types of açaí dietary supplement capsules, ADSC-1 and ADSC-2. The powder obtained from five capsules were extracted with 50 mL methanol twice. The methanol extracts were combined and centrifuged at 4000 rpm at 4 °C for 20 min. The produced supernatant was filtered through 0.45 µm PTFE syringe filters, dried under 295 mbar at 40 °C, and further dried by nitrogen evaporation and lyophilization. The yields were 16.03% (w/w) for ADSC-1 and 13.42% (w/w) for ADSC-2. The prepared extracts will be tested for CYP3A4 inhibition in a subsequent project.

2.2 Determination of absorption profiles of botanicals via passive diffusion

2.2.1 PAMPA assay

All plant extract stock solutions were prepared in PAMPA assay buffer (0.014 M KH_2PO_4, 0.054 M Na_2HPO_4 at pH of 7.4) (Lazaro et al., 2008) with the optimized DMSO concentration.

PAMPA plates pre-coated in structured phospholipids obtained from Corning® Gentest™ (Tewksbury, MA) were stored at -20 °C and warmed to room temperature for 30 min prior to use.

The donor compartment of the 96-well plate apparatus simulated intestinal content pre-absorption, while the acceptor compartment simulated absorbed compounds. A volume of 300 µL of each plant extract solution or standard solution was added to each well in the donor compartment, and 200 µL of the PAMPA assay buffer was added to wells in the acceptor compartment. The plates were then stacked and incubated at room temperature for 5 hrs with shaking at 75 rpm. After incubation, the contents of each well in the donor and acceptor compartments were transferred to the 96-well plates for storage.

2.2.2 Rationale for the extracts' concentrations used in PAMPA and CYP3A4 inhibition/induction assays

A literature search on the human plasma levels of the constituents of açaí and maca found only the plasma concentration of cyanidin-3-O-glucoside in healthy subjects who consumed açaí juice and pulp (Mertens-Talcott et al., 2008). Due to this lack of information, plant extract' concentrations tested were based on the daily dose for açaí and maca BDS on the market. According to the Dietary Supplement Label Database (DSLD) (NIH, 2018), the daily dose for the ingredient form of açaí extract ranges from 15 mg to 6000 mg, while that of maca extract varies from 10 mg to 1500 mg. Intestinal fluid volume (Mudie et al., 2014; Schiller et al., 2005) exhibited individual variability from approximately 20 mL to 180 mL due to food and water intake. To mimic physiological concentrations of the extract in the PAMPA assay, we considered the suggested daily dose of the BDS divided by the estimated intestinal fluid volume (100 mL). Hence, the intestinal concentration can be inferred as 0.15~60 µg/µL for açaí extract and 0.1~15 µg/µL for maca extract. A concentration of 1.5 µg/µL for both extracts was selected for application to the donor compartments for PAMPA assays prior to CYP3A4 induction studies. For CYP3A4 and combined

CYP3A4/5 inhibition studies, the donor compartments had concentration ranges where extracts were soluble to generate the dose-response curves.

2.2.3 Solid phase extraction

A solid-phase extraction cartridge, TARGA C18 column (Part #HMM S18R) from the Nest Group (Southborough, GA), was used to remove salt to combat signal suppression and ionization interferences during LC-MS analysis caused by the phosphate buffer (Sterling et al., 2010). A 100 µL portion from each PAMPA well was desalted through TARGA columns using a well-optimized method (Table 2.1). Each step was accelerated by centrifugation at 1000 rpm for 5 min at 4 °C. Final eluates were dried via nitrogen evaporation, reconstituted in methanol:water (30:70, 0.4% DMSO v/v) and injected into the LC-MS for analysis. MassHunter Qualitative Analysis software ver. B.07.00, MassHunter Mass Profiler B.08.00 and Mass Profiler Professional 14.9 (Agilent Technologies, Inc., Santa Clara, CA) were used for data processing.

Table 2.1. Desalting steps of açaí plant extracts**.**

Desalting steps	**Solvent applied**
Conditioning	200 µL MeOH
Flushing	200 µL H_2O
Equilibration	200 µL H_2O with 2% CAN
Sample loading	100µL sample
Rinsing	200 µL H_2O with 2% CAN
Elution	200 µL 80% MeOH, 0.2% formic acid for 3 times

2.2.4 Chemical fingerprinting by LC-MS

Agilent 6520 Q-TOF mass spectrometer was used for chemical profiling. Methanol açaí extract samples were analyzed on a 4.6 x 100 mm, 3.5 µm ZORBAX Eclipse Plus C18 column (Agilent Technologies, New Castle, DE). The flow rate was set at 0.4 mL/min, the sample injection volume was 5 µL, acquisition rate was set at 1.41 scan/s, and complete mass scanning ranged from *m/z* 100–1000. MS conditions were optimized with a negative ion ESI-MS analysis performed with capillary voltage 3200 V, drying gas temperature 350 °C, fragmentor voltage 175 V, and skimmer 65 V. Nitrogen was supplied as a nebulizing gas at 25 psi and as a drying gas at 10 L/min.

LC separation for methanol açaí extract samples was conducted with a gradient mobile phase consisting of (A) water, 0.1% formic acid and (B) methanol, 0.1% formic acid. The linear gradient was: 0-2 min, 30% B; 25-29 min, 99% B; 30-35 min, 30% B; with 5 min post-time. A time segment from 0 to 20 minutes was set to send the LC flow to the MS detector. Column temperature was set to 40 °C. Negative ESI mode was utilized.

Selected available plant standard compounds were analyzed under the same LC-MS conditions to confirm their presence in the plant extracts.

2.2.5 Structural elucidation by ESI-MS/MS

Targeted MS/MS fragmentation was performed on an Agilent 6520 Q-TOF mass spectrometer. Both MS and MS/MS were set at 1.41 scan/s within the *m/z* range of 100–1000, and collision energies were applied at 5V, 10V, 20V, 30V and 40V. Specifically, for structural elucidation of the five compounds of interest, the parameters were specified in the Table 2.2.

Table 2.2. Parameters of Agilent MassHunter Workstation Data Acquisition for structural elucidation using targeted MS/MS (Seg) mode.

Compound	ESI Mode	Prec. m/z	RT[1] (min)	Delta RT (min)
1	Negative	167.035 $[M - H]^-$	10.8	0.5
2	Negative	359.1511 $[M - H]^-$	11.3	0.6
	Positive	361.1646 $[M + H]^+$	11.3	0.6
		383.1465 $[M + Na]^+$	11.3	0.6
3	Negative	287.0561 $[M - H]^-$	12.92	0.4
4	Negative	331.0833 $[M - H]^-$	16.8	0.6
5	Negative	301.0721 $[M - H]^-$	17.3	0.4

[1] Retention time.

2.3 Determination of CYP3A4 enzyme activity

2.3.1 Calibration curve determination

A matrix-matched product calibration curve using $^{13}C_3$ 1′-hydroxymidazolam as isotope labelled internal standard was run in roughly the same reaction matrices as inhibition assay (as stated in 2.3.3), except that PAMPA buffer was used in place of plant extracts from PAMPA assay, and the substrate midazolam was replaced by a range of 0.25, 0.5, 0.75, 1.0, 1.25, 1.5, 1.75, 2.0, 2.25, 2.5 µM of 1′-hydroxymidazolam standard compound. To avoid saturation of LC/MS, the matrices were diluted for 10 times before injection. This calibration curve was further used to calculate limit of detection (LOD) and limit of quantification (LOQ).

2.3.2 Solvent optimization

The impact of DMSO to CYP3A4 and CYP3A4/5 activities was evaluated to avoid DMSO-induced decrease in sensitivity of enzyme activity assay. A range of 0%, 0.5%, 1%, 1.5%, 2%, 2.5%, 3%, 4% and 5% of DMSO was spiked in PAMPA buffer, and incubated with pooled or genotyped HLM, midazolam stock solution and NADPH following by quench and dilution (as stated in 2.3.3). The production of 1′-hydroxymidazolam was quantified by LC-MS.

2.3.3 CYP3A4/5 enzyme activity assay

As shown in Fig. 1.1, CYP3A4/5 enzymatic reaction matrices contained plant extracts from PAMPA assays and 0.2 mg/mL pooled HLM in inhibition buffer (5 mM $MgCl_2$ and 1 mM EDTA in 100 mM potassium phosphate buffer at pH 7.4). Ketoconazole at 10 µM was used as a positive control in place of plant extract, while DMSO control from PAMPA plates was used as a negative control to delineate the inhibition effect of plant extracts from DMSO. Midazolam stock solution

prepared in methanol:buffer (30:70 v/v) was added at its Km concentration (3 µM) (Yuan et al., 2002). Enzymatic reaction mixtures were pre-incubated at 37 °C for 5 minutes with shaking at 75 rpm, after which the reactions were initiated by addition of 1 mM NADPH and incubated at 37 °C with shaking at 75 rpm for an optimized incubation time of 10 minutes. Reactions were stopped by adding 20 µL water/acetonitrile (ACN) /formic acid (92:5:3, v/v/v) with stable isotope labelled internal standard ($^{13}C_3$ 1′-hydroxymidazolam, 1.0 µM) to minimize the error generated from dilution bias. Reaction mixtures were then vortexed for 1 min and centrifuged at 13,000 x g at 4 °C for 15 min. The supernatant was 10-fold diluted and injected into the LC-MS to monitor the production of metabolite 1′-hydroxymidazolam.

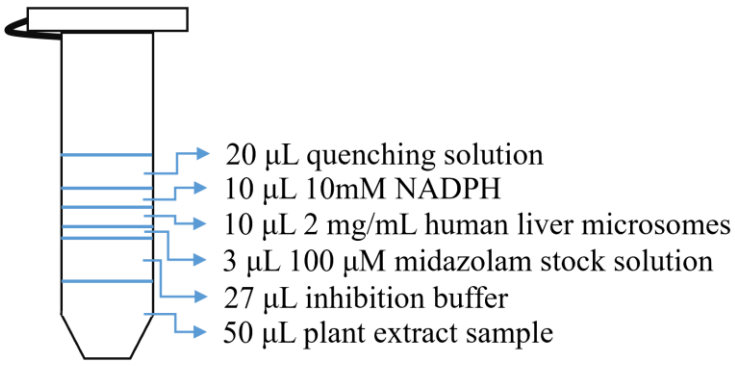

Figure 1.1. Schematic representation of CYP3A4/5 inhibition assay.

Once the potential (>50%) CYP3A4 inhibition was obtained by açaí and maca plant extracts, half maximal inhibitory concentration (IC_{50}) was determined to analyze the inhibitor's potency. This was determined through incubation mixtures with 2-fold increasing concentrations of the plant extract that covered the concentrations assayed in the initial CYP3A4 inhibition screening.

Agilent 6520 Q-TOF mass spectrometer with a 1220 rapid resolution liquid chromatography (RRLC) system (Agilent Technologies, Little Falls, DE) was used for quantitation of 1′-

hydroxymidazolam on a 4.6 x 100 mm, 3.5 µm ZORBAX Eclipse Plus C18 column. The flow rate was set at 0.4 mL/min, and the sample injection volume at 1 µL while the acquisition rate was 1.41 scan/s with the complete mass scanning range from *m/z* 100–1000. The MS conditions were optimized with a positive mode electrospray (ESI)-MS analysis performed at a capillary voltage 3200 V, drying gas temperature 350 °C, fragmentor voltage 175 V and skimmer 65 V. Nitrogen was supplied as a nebulizing gas at 25 psig and as a drying gas at 10 L/min. LC conditions consisted of a gradient mobile phase with (A) water containing 0.1% formic acid and (B) methanol. The optimization was set to a 4 min gradient from 75% to 100% of solvent B followed by a 1 min post-run of 75% B with a flow rate of 0.4 mL/min and a column temperature of 40 °C. Detection was in positive ESI mode.

Quantitative LC-MS data were analyzed using MassHunter Quantitative Analysis software and MassHunter Qualitative Analysis software ver. B.07.00 (Agilent Technologies, Inc., Santa Clara, CA). The ratio of the peak areas of compounds produced by LC-MS and other calculations were performed using Microsoft Excel (Seattle, WA). GraphPad Prism 5.02 software (GraphPad Software Inc., San Diego, USA) was used to generate the log dose-response curves and IC_{50} values.

2.3.4 Specific CYP3A4 enzyme activity assay

The inhibition assay described above was followed with the exception that genotyped HLM (CYP3A5 NULL) was used in place of pooled HLM.

2.4 Determination of CYP3A4 gene expression level

2.4.1 Culture of human primary hepatocytes

The hepatocytes were cultured by following a published protocol (Pondugula et al., 2015b) (Abbott et al., 2019). Briefly, the hepatocytes were incubated for 4 hr in the plating media in collagen coated 24-well culture plates in an atmosphere of 5% CO_2 at 37°C. The plating media was then aspirated, and the cells were incubated in the maintenance media for 6 h. The hepatocytes were then treated with the vehicle (DMSO negative control), rifampicin (RIF, positive control), or extracts in the maintenance media for 24 hr before harvesting total RNA for gene expression studies.

2.4.2 RNA isolation

Total RNA was extracted from the human primary hepatocytes using the E.Z.N.A. Total RNA Kit I (Omega Bio-Tek). The quality and quantity of the total RNA was assessed using a NanoVuePlus Spectrophotometer (GE Healthcare). Reverse transcription was performed with the iScript cDNA Synthesis Kit (Bio-Rad).

2.4.3 Quantitative RT-PCR analysis

Quantitative polymerase chain reaction (qPCR) was performed using the PerfeCTa SYBR Green FastMix (Quanta BioSciences) and CFX96 Touch Real-Time PCR Detection System (Bio-Rad). Transcripts of the housekeeping gene 18S rRNA and CYP3A4 were amplified using the gene-specific primers (Table 2.3). The comparative C_t method was used for relative quantification for gene expression.

Table 2.3. Forward (F) and reverse (R) primers used for quantitative RT-PCR of 18S rRNA and CYP3A4.

Gene/Primer sequence	Amplified segment (bp)	Gene Bank Accession no
18S rRNA F: 5'-GAGGTTCGAAGACGATCAGA-3' R: 5'- TCGCTCCACCAACTAAGAAC-3'	315	BK000964
CYP3A4 F: 5′- TTGGAAGTGGACCCAGAAAC -3′ R: 5′- CTGGTGTTCTCAGGCACAGA -3′	265	NM_017460

2.4.4 Cell viability assay

Human colon cancer cells (LS174) were seeded into 96-well culture plates (PerkinElmer), followed by incubation with the vehicle (DMSO or RIF in buffer) or the extracts for 20 hr. By performing CellTiter-Glo luminescent cell viability assays (Promega), then cell viability was determined by quantifying the amount of ATP which reflects the presence of metabolically active cells. Luminescence was measured with a FLUOstar Optima microplate reader (BMG Labtech). (Pondugula et al., 2015a)

2.5 Determination of liver metabolism of botanicals or standard compounds

2.5.1 Liver UGT metabolism assay

This assay was developed to access the identities of the live UGT-mediated metabolites. To allow pore formation in the microsomes, 10 mg/mL pooled HLM was activated by 50 µg/µl alamethicin on ice for 15 minutes (Fisher et al., 2000). Then it was added into the reaction matrix (Fig 1.2), resulting in a mixture containing 5 mM saccharolactone, 50 µM tested standard compound and 1 mg/mL activated HLM in metabolic buffer (5 mM $MgCl_2$ and 1 mM EDTA in 100 mM potassium phosphate buffer at pH 7.4). This matrix was pre-incubated at 37 °C for 5 minutes with shaking at 75 rpm, after which the reactions were initiated by addition of 5 mM UDPGA and incubated at 37 °C with shaking at 75 rpm for 30 minutes. Reactions were stopped by centrifugation at 13,000 x g at 4 °C for 15 min. The supernatant was injected into the LC-MS to monitor the formation of metabolites.

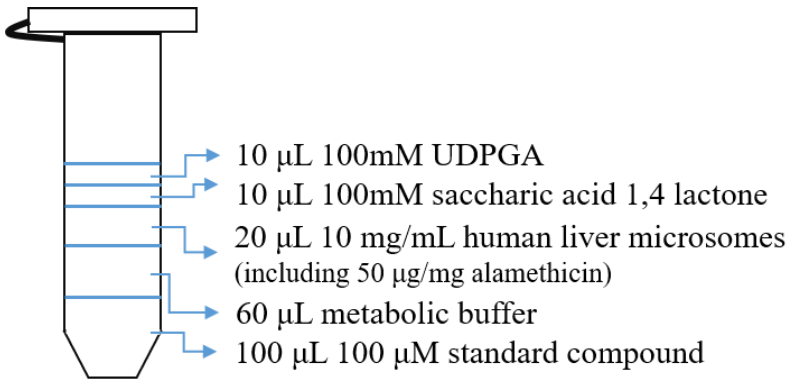

Figure 1.2. Schematic representation of liver UGT assay.

2.5.2 Liver CYP metabolic assay

This assay was developed to identify the live CYP-mediated metabolites. As shown in Fig. 1.3, the reaction matrix containing 50 µM tested standard compound and 1 mg/mL HLM in metabolic buffer was pre-incubated at 37 °C for 5 minutes with shaking at 75 rpm, after which the reactions were initiated by addition of 1 mM UDPGA and incubated at 37 °C with shaking at 75 rpm for 30 minutes. Reactions were stopped by centrifugation at 13,000 x g at 4 °C for 15 min. The supernatant was injected into the LC-MS to monitor the formation of metabolites.

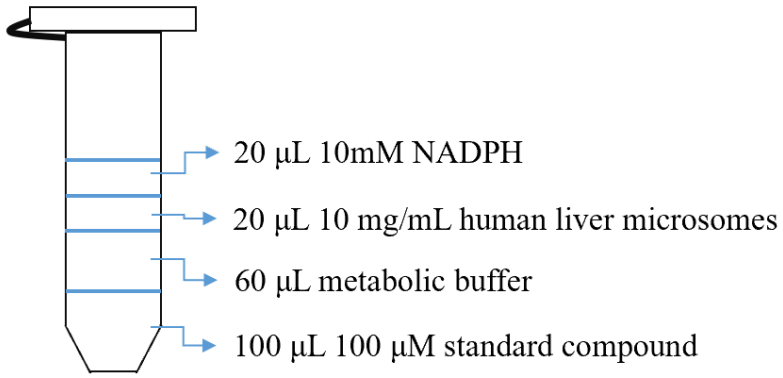

Figure 1.3. Schematic representation of liver CYP assay.

Chapter 3: Results and discussion

3.1 Evaluation of the impact on CYP3A4 enzyme activities

3.1.1 Optimization of DMSO concentration for inhibition assays

To avoid DMSO-induced potential reduction of enzyme activity in the inhibition assay (Chefson and Auclair, 2007), the concentration of DMSO to dissolve plant extracts was optimized. Fig. 2.1 and Fig. 2.2 are the summary results from the DMSO inhibition assay. The production of 1′-hydroxymidazolam decreased linearly with an increase in DMSO concentration. The efficiency of midazolam 1′-hydroxylation catalyzed by combined CYP3A4/5 was decreased by 6.53% upon addition of 0.1% DMSO and by 8.71% with 0.15% DMSO. However, CYP3A4 activities were decreased by 9.02% and 12.40% separately upon the use of 0.1% and 0.15% DMSO. Therefore, DMSO concentration in the incubation mixture for inhibition assays should be below 0.125% to control its inhibiting effect to less than 10%. Considering the equilibration of chemicals (i.e., DMSO) via passive diffusion during PAMPA incubation, 0.208% of DMSO in PAMPA donor compartment before incubation guarantees that the acceptor compartment received less than 0.125% DMSO. This rationale was confirmed by the supplier of PAMPA plates, Corning® Gentest™. Thus, plant extracts were dissolved in 0.208% DMSO for all samples in the PAMPA assays. The suitability of DMSO concentrations to dissolve the plant extracts was observed and confirmed in the following experiments.

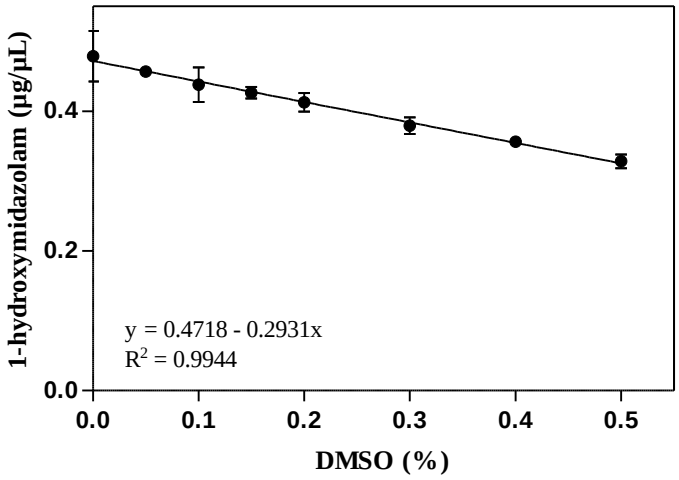

Figure 2.1. Effect of DMSO (v/v, %) in phosphate buffer (pH=7.4) on midazolam 1′-hydroxylation catalyzed by combined CYP3A4/5 using pooled HLM. Data expressed as mean ± SD of three independent experiments.

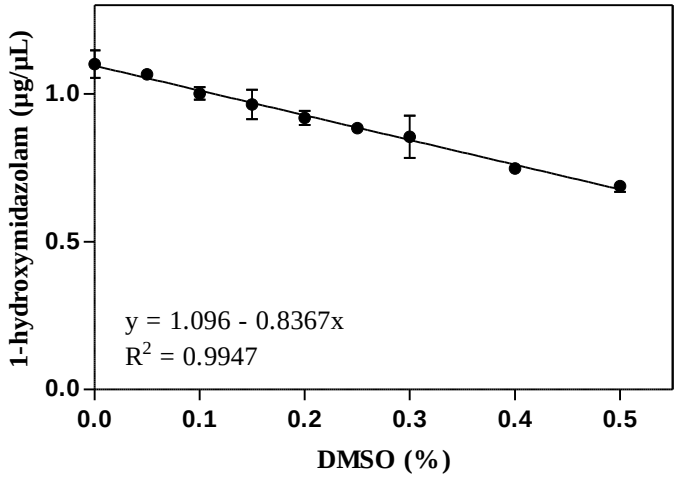

Figure 2.2. Effect of DMSO (v/v, %) in phosphate buffer (pH=7.4) on midazolam 1′-hydroxylation catalyzed by CYP3A4 using genotyped HLM. Data expressed as mean ± SD of three independent experiments.

3.1.2 Evaluation of the impact on CYP3A4/5 enzyme activities by passively diffused constituents in açaí and maca

For methanol and acidic methanol extracts of açaí and maca, passively diffused compounds obtained from the acceptor compartment of the PAMPA plate displayed a dose-response relationship producing 50% CYP3A4/5 inhibition (Fig. 3.1) at donor compartment concentrations from 20.18 µg/µL to 57.92 µg/µL. Distinctive inhibitory effects were detected in the four tested extracts. Methanol extracts of both açaí and maca generally displayed higher inhibition potential than acidic methanol extracts. Passively diffused compounds in the methanol açaí extract displayed the highest inhibitory effect showing 50% CYP3A4/5 inhibition at donor compartment concentrations of the extracts of 20.18 µg/µL. IC_{50} values reported for passively diffused açaí and maca constituents in the acceptor compartments for CYP3A4/5 inhibitory activity were calculated based on the concentrations of the extracts applied on the donor compartments of the PAMPA plates at time 0. These values do not reflect the concentration in the acceptor compartment.

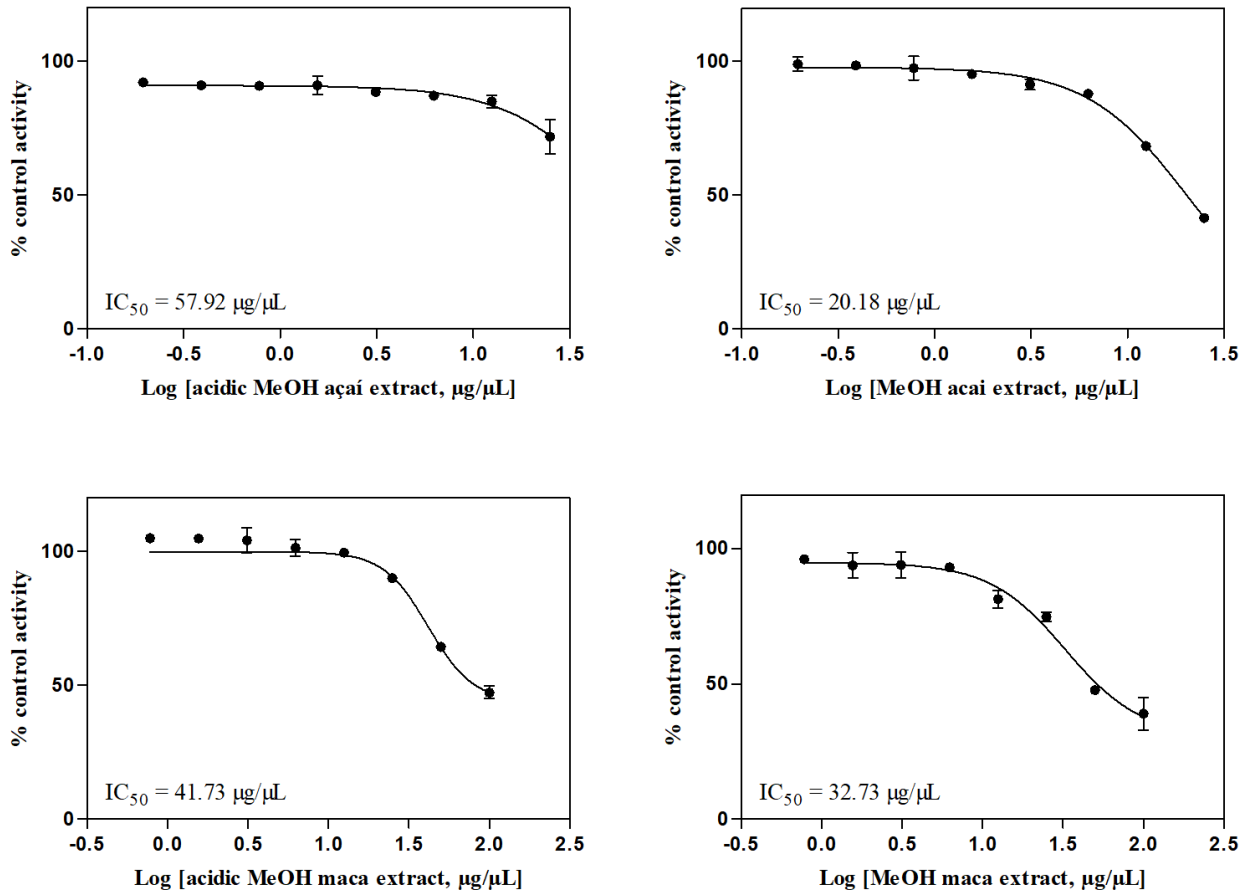

Figure 3.1. Inhibition curves for the inhibition of combined CYP3A4/5 enzymes by passively diffused compounds in açaí and maca extracts. Activity expressed as the percentage of the remaining activity compared with DMSO control. Ketoconazole control was used to define the bottom plateau of the curves. Data expressed as mean ± SD of three independent experiments. IC_{50} values were calculated based on concentrations of PAMPA donor compartment at time 0.

3.1.3 Evaluation of the impact on CYP3A4 enzyme activities by passively diffused and non-passively diffused constituents in açaí and maca

The inhibition potential of all extracts on CYP3A4 were then evaluated. As another CYP isoform, CYP3A5 plays a relatively minor role in anticancer drug metabolism compared to CYP3A4 (Dennison et al., 2006; Li et al., 2007; Nebot et al., 2010; Santos et al., 2000; Shou et al., 1998; Zhuo et al., 2004), and its genetic expression is varied across populations (Williams et al., 2003). Delineation of the role of CYP3A4 from CYP3A5 is quite challenging (Walsky et al., 2012) because of the significant overlapping substrate specificity and different metabolic pattern (Emoto and Iwasaki, 2006). Expressed CYP3A5 activity is largely determined by allele CYP3A5*3, which causes alternative splicing and results in truncated non-functional enzymes. Furthermore, homozygous carriers of CYP3A5*3/*3 did not express any CYP3A5 enzyme activity (Roy et al., 2005; Zaltzman et al., 2016). Therefore, CYP3A4 inhibition assay based on polymorphic genotyped CYP3A5*3/*3 HLM was deployed to exclude the effects of CYP3A5, and the corresponding parameters of selectivity and sensitivity were determined (Table 3.1). The inhibition curves displayed in Fig. 3.2 showed the same trend. In addition, the inhibition potential of non-passively diffused compounds was investigated. The same trend was observed in inhibition potentials. The non-passively diffused compounds in acidic methanol açaí extract exhibited the highest inhibitory activities.

Table 3.1. Parameters of calibration curves, LOD and LOQ of 1′-hydroxymidazolam in two CYP3A4 inhibition assays.

	Linear range (μM)	Weighting factor	Slope (a)	Intercept (b)	Coefficient of determination	LOD (μM) [1]	LOQ (μM) [2]
Combined CYP3A4/5 inhibition assay	0.2867-2.8674	None	1.1005	0.1215	0.9988	0.0121	0.0404
CYP3A4 inhibition assay	0.1843-1.8433	None	0.8234	0.1262	0.9925	0.0164	0.0547

[1, 2] Values were calculated from n = 5 repetitive measurements. The limit of detection (LOD) and the limit of quantitation (LOQ) were calculated as follows: $LOD = \frac{3\sigma}{a}$, $LOQ = \frac{10\sigma}{a}$ where a is the slope of the calibration curve, and σ is the standard deviation of the standard compound at the lowest concentration level.

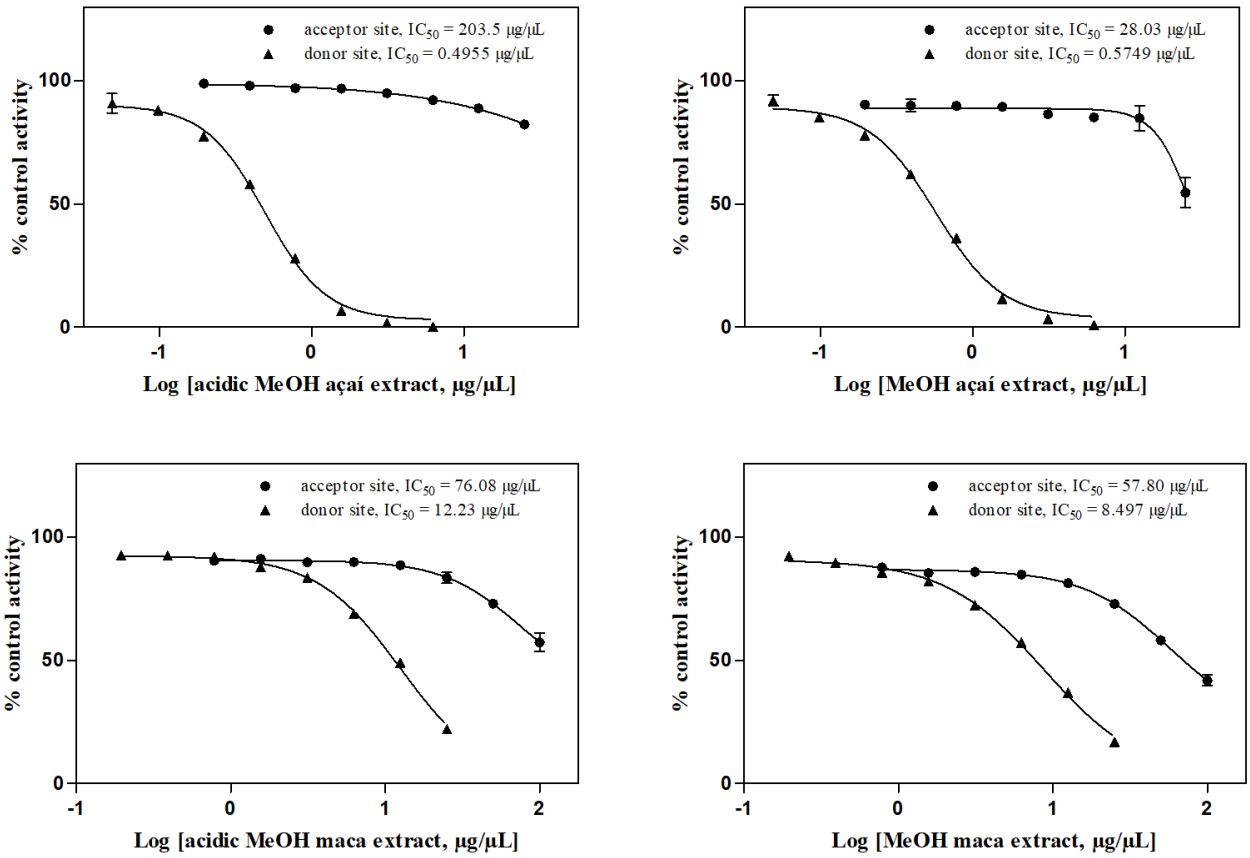

Figure 3.2. Inhibition curves for the inhibition of CYP3A4 by non-passively diffused (from PAMPA donor compartment) and passively diffused (from PAMPA acceptor compartment) compounds in açaí and maca extracts. Activity expressed as the percentage of the remaining activity compared with DMSO control. Ketoconazole control was used to define the bottom plateau of the curves. Data expressed as mean ± SD of three independent experiments. IC_{50} values were calculated based on concentrations of PAMPA donor compartment at time 0.

3.2 Evaluation of the impact on CYP3A4 gene expression level

3.2.1 Evaluation of the impact on CYP3A4 gene expression level by plant constituents

The initial induction assay (Fig. 3.3) was set for screening of plant extracts for their CYP3A4 induction potential in human primary hepatocytes. As expected, RIF strongly induced CYP3A4 mRNA expression. Slight CYP3A4 induction was found with maca extracts. CYP3A4 mRNA levels were significantly increased with açaí extracts, suggesting the presence of CYP3A4 inducers in açaí extracts.

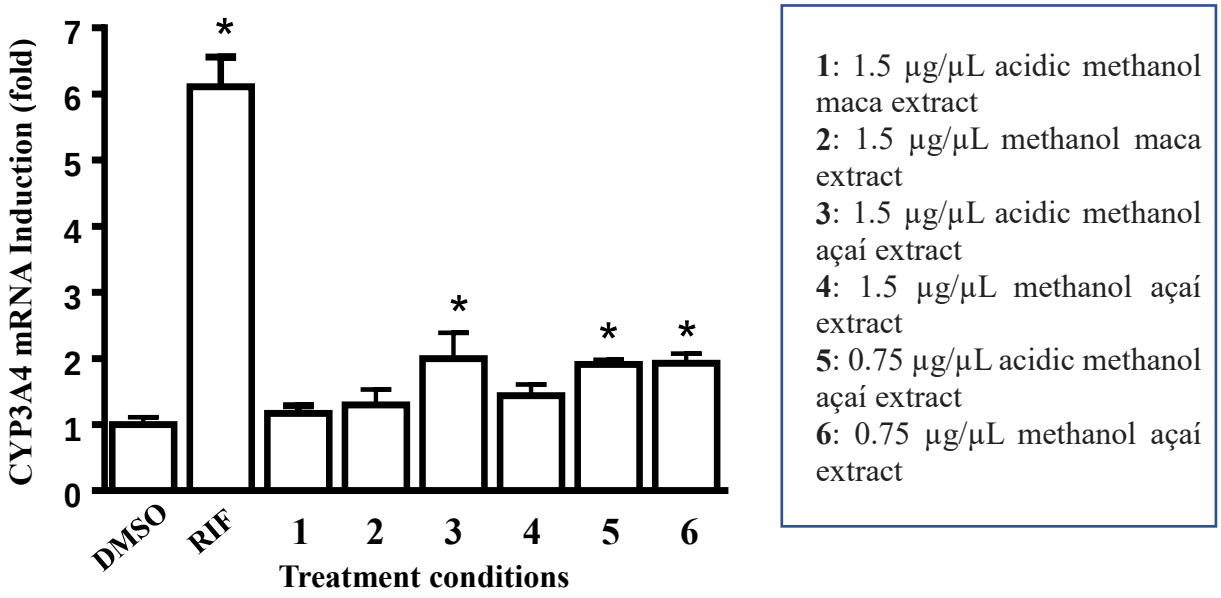

Figure 3.3. Compounds in açaí and maca extracts in PAMPA donor compartment at time 0 that induced CYP3A4 gene expression in human primary hepatocytes. Results are fold increase over the DMSO control, and data are expressed as mean values ± SD of three independent experiments. Statistical significance (*, $p<0.05$) was determined by analysis of variance (ANOVA) with Dunnett's multiple comparisons test.

3.2.2 Evaluation of the impact on CYP3A4 gene expression level by passively diffused plant constituents

Induction potential of the passively diffused compounds was then determined for the tested extracts (Fig. 3.4) using the PAMPA model to simulate passive intestinal absorption.

A significant increase of CYP3A4 mRNA expression was identified in the hepatocytes treated with the solution from acceptor compartments of PAMPA plates containing methanol açaí extracts, while passively diffused compounds of acidic methanol açaí extracts exhibited minor inhibitory activities. However, no significant induction or inhibition was observed with passively diffused constituents of maca extracts.

Notably, while some compounds may induce CYP (Pondugula et al., 2015b), others in the same extract dmay repress it (Abbott et al., 2019). It is possible that the compounds profile in the passively diffused extract is different from that of the donor extract in that repressors are missing after passive diffusion, resulting in net induction effect. This could explain the fact that the net effect of all compounds in methanol açaí at 1.5 µg/µL was not significant, whereas the passively diffused proportion induced the expression of CYP3A4 mRNA.

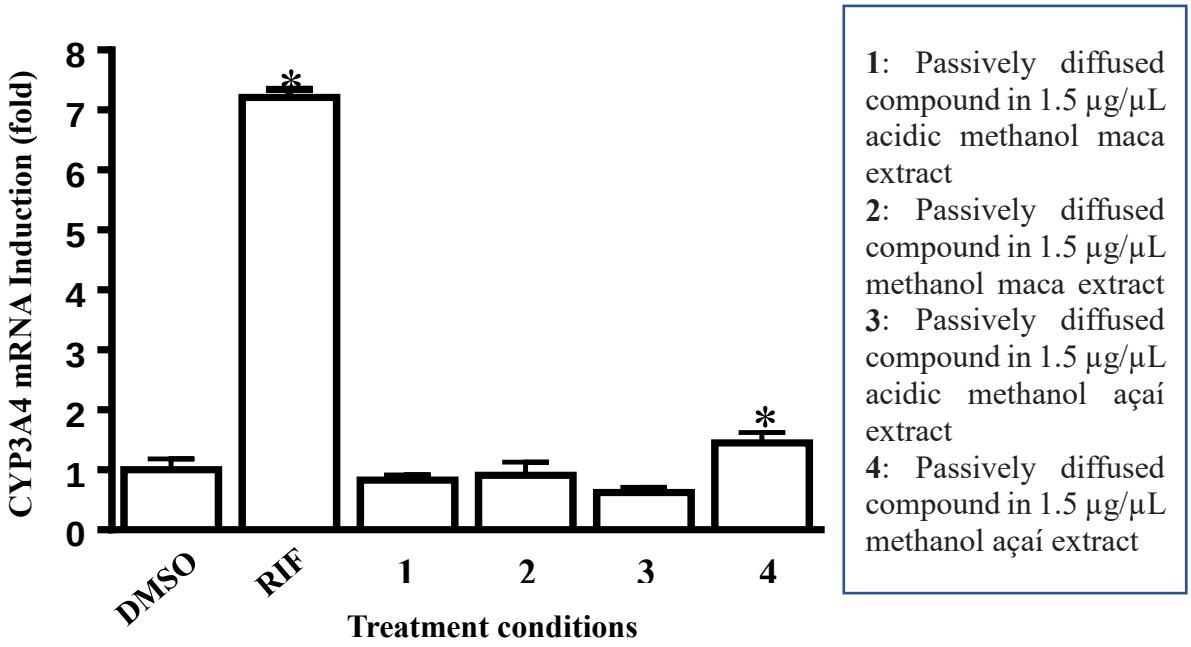

Figure 3.4. Passively diffused compounds in açaí and maca extracts altered CYP3A4 gene expression in human primary hepatocytes. Results are fold change over the DMSO control, and data are expressed as mean ± SD of three independent experiments. Statistical significance (*, $p<0.05$) was determined by ANOVA with Dunnett's multiple comparisons test.

3.2.3 Evaluation of cytotoxicity

In CellTiter-Glo Luminescent Cell Viability Assays, our preliminary data (Fig. 3.5) showed that both methanol açaí extracts and acidic methanol açaí extracts exhibited significant cytotoxicity at 1.5 μg/μL and 0.75 μg/μL. In contrast, co-culture with methanol maca extract significantly increased the viability of LS174 cells, which indicates that the components in methanol maca extract can potentially promote cell proliferation. Exposure to acidic methanol extract did not affect the cell viability significantly.

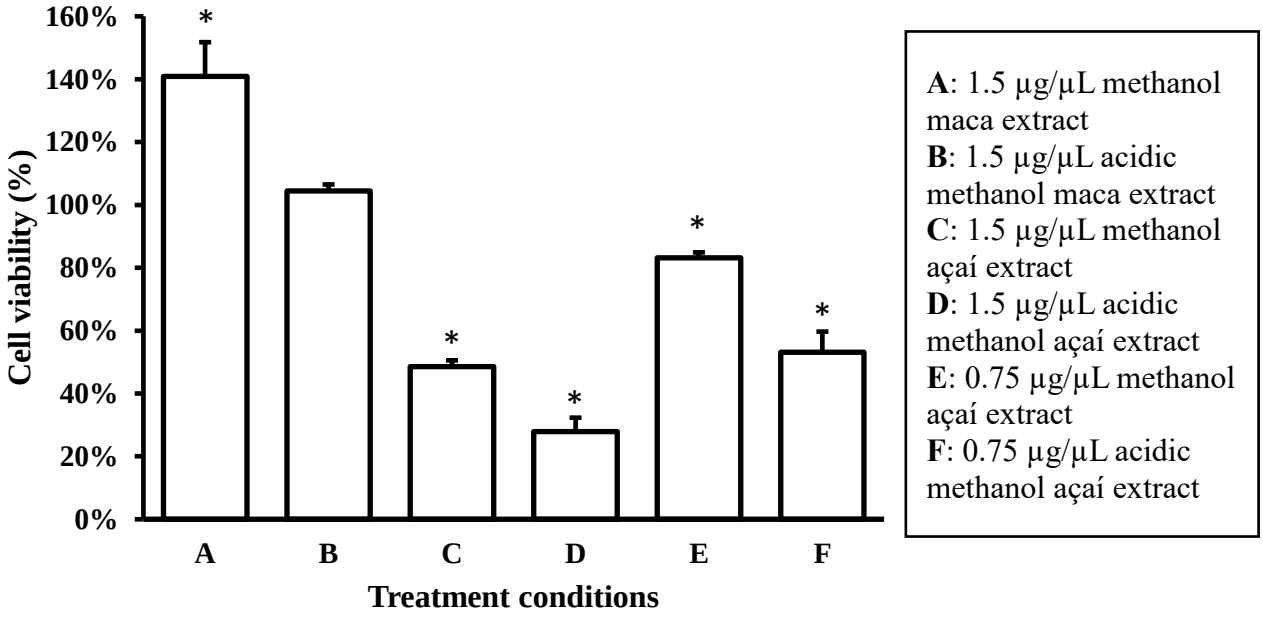

Figure 3.5. Compounds in açaí and maca extracts in the PAMPA donor compartment at time 0 influenced the viability of LS174 cells after 20 hr treatment. The viability of vehicle (DMSO) treated cells was expressed as 100% (not shown). Data are expressed as mean values ± SD of three independent experiments. The statistical significance (*, $p<0.05$) was determined by student's t test.

To further investigate the cytotoxicity caused by açaí extracts, the viability of LS174 cells was determined after incubation for 20 hr with passively diffused and non-passively diffused compounds of açaí extracts obtained from the PAMPA plate (Fig. 3.6). Surprisingly, significant change in cell viability was only found in the treatment which exposed the cell to passively diffused compounds from methanol açaí extracts, which gave a strong increase in cell viability. In other treatments, the cell viability was decreased. This phenomenon indicated that most of the potential cytotoxic components in açaí extracts were of relatively low permeability and remained in the PAMPA donor compartment after 5 hrs incubation. Further studies may be done to validate the data by increasing the concentration in donor compartment (time 0) of the PAMPA assay to 1.5 µg/µL.

The cell viability assay data may be useful to explain some of our previous findings. For methanol açaí extract in the PAMPA donor compartment at time 0 (Fig 2.1), a lower concentration of extract (0.75 µg/µL) exhibited more induction potential compared to a higher concentration (1.5 µg/µL). This discrepancy in induction potential could result from the high cytotoxicity of concentrated methanol açaí extract. Metabolic inactive hepatocytes would stop synthesis of mRNA, leading to a decreased mRNA expression. However, further cell viability studies on normal hepatocyte cell lines would be necessary to confirm this assumption.

Furthermore, our findings were consistent with the literature data. For example, resveratrol, a mid-polar compound in açaí berries, has been reported to have strong cytotoxicity in cell lines. In addition, two açaí constituents, (+)-7*S*8*R*-7′,8′-dihydroxy-dihydrodehydroconiferyl alcohol-9-*O*-β-d-glucopyranoside and 4-hydroxy-2-methoxyphenyl 1-*O*-[6-(hydrogen 3-hydroxy-3-methylpentanedioate)]-β-d-glucopyranoside, were determined to have cytotoxic effects on HL-60

cells (Hu et al., 2014). On the other hand, many studies affirmed the idea that the components of maca extract possess none or subtle significant cytotoxic effects (Xia et al., 2018; Yu et al., 2017).

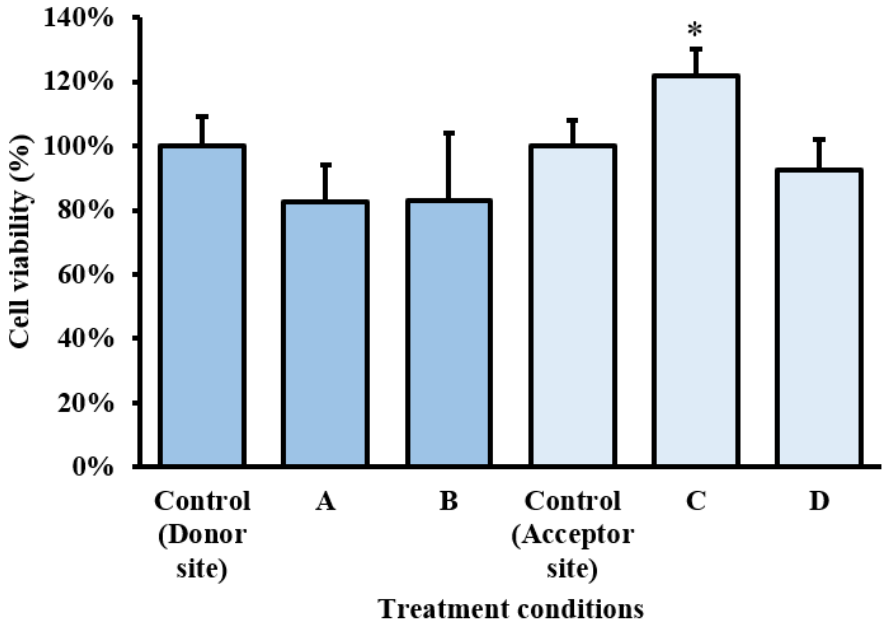

A: Non-passively diffused compound in 0.75 µg/µL methanol açaí extract
B: Non-passively diffused compound in 0.75 µg/µL acidic methanol açaí extract
C: Passively diffused compound in 0.75 µg/µL methanol açaí extract
D: Passively diffused compound in 0.75 µg/µL acidic methanol açaí extract

Figure 3.6. Passively diffused and non-passively diffused compounds in açaí and maca extracts influenced the viability of LS174 cells after 20 hr treatment. The viability of vehicle (passively diffused and non-passively diffused DMSO) treated cell was expressed as 100% (not shown). Data are expressed as mean values ± SD of three independent experiments. Statistical significance (*, $p<0.05$) was determined by student's *t* test.

3.3 Determination of absorption profile via passive diffusion

3.3.1 Calculation for passive permeability

Effective passive permeability (P_e) values were calculated using the following formula:

$$P_e = \frac{-\ln[1-\frac{C_A(t)}{C_{equilibrium}}]}{A\times(\frac{1}{V_D}+\frac{1}{V_A})\times t} \quad (1)$$

Where $C_{equilibrium}$ was the concentration of the compound in both donor and acceptor compartments at equilibrium:

$$C_{equilibrium} = \frac{[C_D(t)\times V_D + C_A(t)\times V_A]}{V_D+V_A} \quad (2)$$

A was the membrane area (0.3 cm^2); t was the incubation time (18000 s); $C_D(t)$ and $C_A(t)$ represented the concentration of compound of interest in donor or acceptor compartment at time t, respectively; V_D and V_A were the volume of solution applied in the donor compartment (0.3 cm^3) and acceptor compartment (0.2 cm^3).

3.3.2 Mass Profiler Professional (MPP) introduction

Agilent Mass Profiler Professional software is a powerful chemometric tool for mining MS-based data. It uses approaches including principle component analysis (PCA), significance analysis (e.g. t-test, ANOVA, etc.) and ID browser identification to access MS data. Furthermore, MPP can be utilized for various purposes, including metabolomics studies (Gu et al., 2011; Musharraf et al., 2015; Vizcaino and Crawford, 2016), food authentication (Avula et al., 2015) and wine classification (Vaclavik et al., 2011).

3.3.3 MPP-based chemometric analysis

Previously, Awortwe et al. (2014) used the PAMPA assay prior to the assessment of major metabolizing CYPs inhibitory activity of botanicals. We have developed a more informative strategy to target passively diffused constituents for interference of CYP3A4. Our strategy also allows for the MS-based identification of the bioactive compounds.

In addition to compounds selected based on the high abundance in PAMPA acceptor compartment in methanol açaí extract samples, those with high permeability should be considered because of their likelihood for absorption. To screen the compounds with high permeability, Mass Profiler coupled with MPP was used for the first time in a permeability study. After batch recursive feature extraction and data alignment, a total of 846 entities among sample groups (including donor compartment after 5 hs incubation, acceptor compartment after 5 hs incubation, and control group) were extracted. Additionally, by applying a filter of frequency of occurrence and a Venn diagram to exclude the background ions introduced during sample preparation (Fig. 4.1), 43 entities that reached the acceptor compartment were selected for focused study. Furthermore, a restriction of fold change (FC) between compound abundance in donor and acceptor compartments after 5-hr incubation was employed to select compounds with high permeability. The boundary line was based on a predicted fraction absorbed of 30%, or a log P_e value of -4.70, which was considered an acceptable starting point for predicting absorption and the cutoff between low and high passive permeability in many studies (Matsson et al., 2005; Petit et al., 2016). As this value converted to a FC of 2.146 under our PAMPA model, 3 out of 43 entities with a FC less than or close to this value were extracted (Table 3.2). Moreover, together with the compounds of high abundance in the acceptor compartment, five compounds were identified as likely absorbable compounds with the potential to produce CYP3A4-mediated drug-botanical interactions. Fig. 3.7 and Fig. 3.8

display the effective passive permeability and the relative abundance of the five compounds of interest.

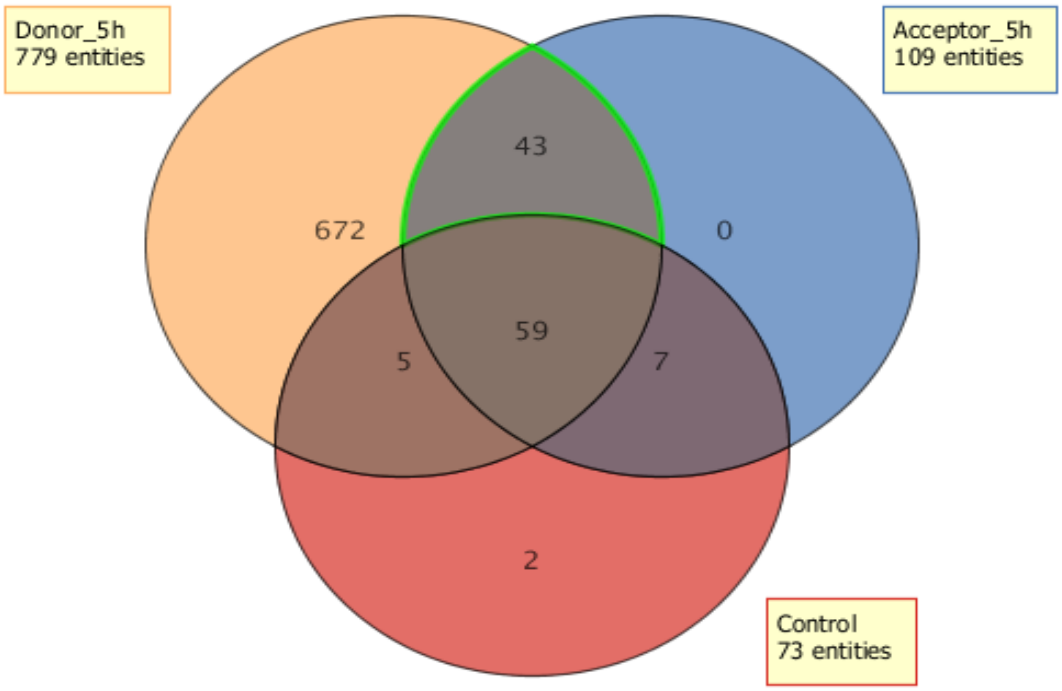

Figure 3.7. Venn diagram of methanol açaí extract compounds present in control and in PAMPA donor/acceptor sites after 5 hrs incubation. Compounds present in control group were excluded from analysis; 43 out of 779 compounds (highlighted in green) passively diffused through the membrane.

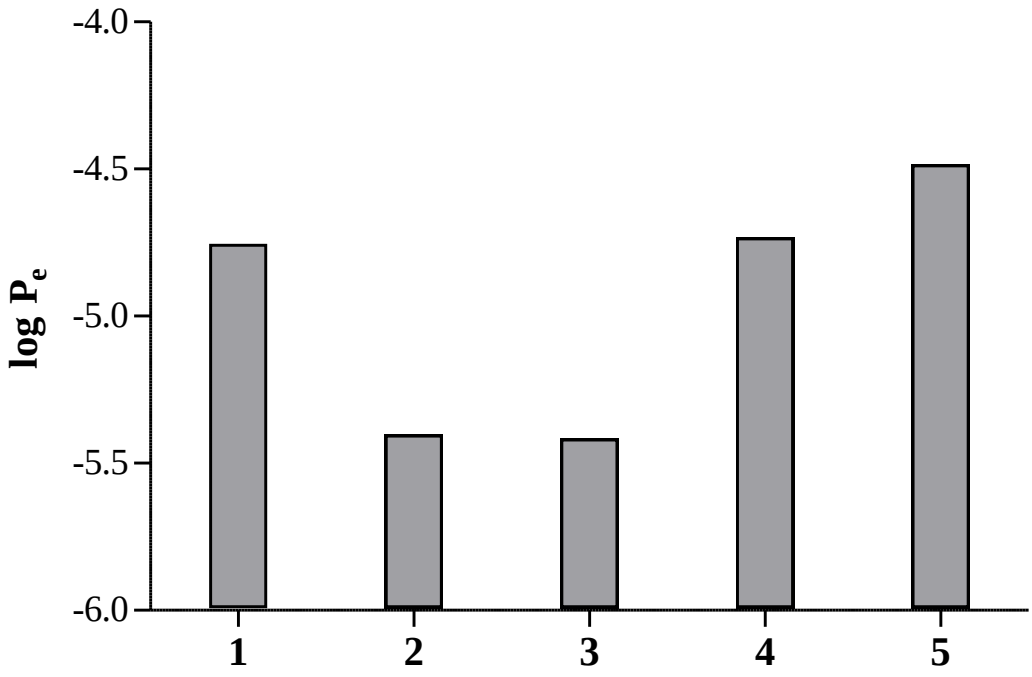

Figure 3.8. Comparison of calculated effective passive permeability of açaí compounds of interest.

Table 3.2. Compounds characterized by high permeability.

Compound	Averaged measured molecular mass (Da)	Averaged measured retention time (min)	Fold change ([donor_5h] vs [acceptor_5h]) [1]
5	302.0799	17.189	1.47
1	168.042	10.669	2.26
4	332.0899	16.785	2.34

[1] Normalized.

3.3.4 Identification compounds with highest abundance or permeability

Methanol açaí extract showed the highest CYP3A4 inhibition and induction potential. Therefore, five compounds characterized by high abundance or high permeability were selected in methanol açaí extract appear in the LC-MS chromatogram in Fig. 3.9, and further elucidated by MS and tandem mass spectrometry (MS/MS). The assigned formula, retention time, MS and MS/MS data are shown in Table 3.3, and the chemical structures of bioactive compounds are presented in Fig 3.10. Compound **1**, compound **3** and compound **5** were confirmed by comparison with their standard compounds, while compound **2** was assigned by comparison with the reported MS/MS fragmentation pattern of corresponding standard compound. Compound **4**'s structure was inferred from its fragmentation pattern.

Table 3.3. Retention times and mass spectral data of the five açaí compounds.

	RT[1] (min)	Accurate mass $[M-H]^-$	Exact mass $[M-H]^-$	Assigned formula	DBE[2]	Error (ppm)	Score	MS/MS *m/z* (% base peak)	Assigned compound identification
1	10.72	167.0348	167.035	$C_8H_8O_4$	5	1.3	99.21	10 eV CE[3]: 167 (100), 108 (27), 152 (15); 20 eV CE: 108 (100), 167 (8); 30 eV CE: 108 (100).	protocatechuic acid methyl ester
2	11.26	359.1511	359.15	$C_{20}H_{24}O_6$	9	-2.98	96.34	10 eV CE: 359 (100), 344 (10); 20 eV CE: 344 (100), 359 (56), 313 (16), 329 (15); 30 eV CE: 241 (100), 109 (97), 344 (96), 313 (84), 299 (80), 255 (67), 329 (53), 314 (44), 159 (37), 173 (36).	isolariciresinol
3	13.29	287.0568	287.0561	$C_{15}H_{12}O_6$	10	-2.36	96.99	10 eV CE: 287 (100), 259 (71), 125 (19); 20 eV CE: 125 (100), 259 (47), 152 (14), 151 (12), 177 (12), 243 (11); 30 eV CE: 125 (100), 177 (28).	dihydrokaempferol
4	16.81	331.0824	331.0823	$C_{17}H_{16}O_7$	10	0.66	89.88	10 eV CE: 331 (100); 20 eV CE: 151 (100), 331 (73), 179 (33), 164 (30), 316 (21), 164 (14); 30 eV CE: 151 (100), 164 (74), 164 (64), 136 (47), 107 (42), 149 (36), 179 (28).	5,7-dihydroxy-2-(4-hydroxy-3,5-dimethoxyphenyl)-2,3-dihydro-4H-chromen-4-one
5	17.22	301.0725	301.0718	$C_{16}H_{14}O_6$	10	-1.82	97.89	10 eV CE: 301 (100), 151 (9); 20 eV CE: 151 (100), 301 (47), 149 (36), 164 (17), 134 (15), 107 (15); 30 eV CE: 134 (100), 151 (75), 107 (47), 164 (41), 149 (40), 136 (32).	homoeriodictyol

[1] Retention time.
[2] Double bond equivalent.
[3] CE: collision energy

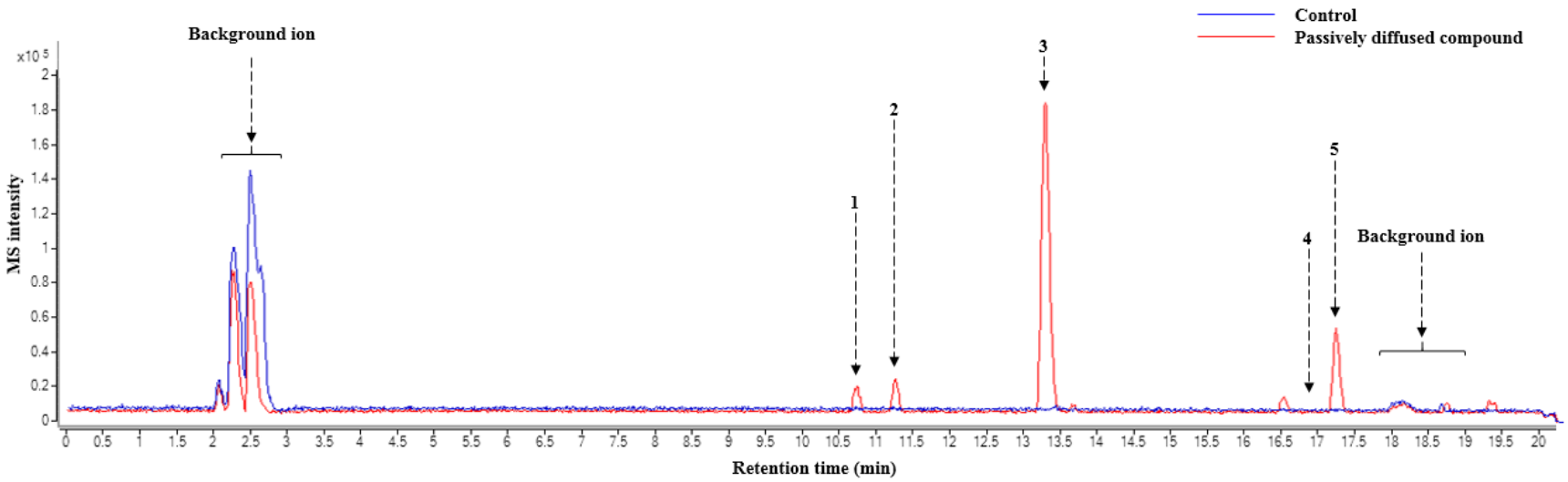

Figure 3.9. Comparison of chromatography of passively diffused compounds in methanol açaí extract with control. Compounds of interest are numbered from 1~5, among which Compound **1**,**2**,**3**,**5** are characterized by high abundance, while Compound **1**,**4**,**5** are characterized by high passive permeability.

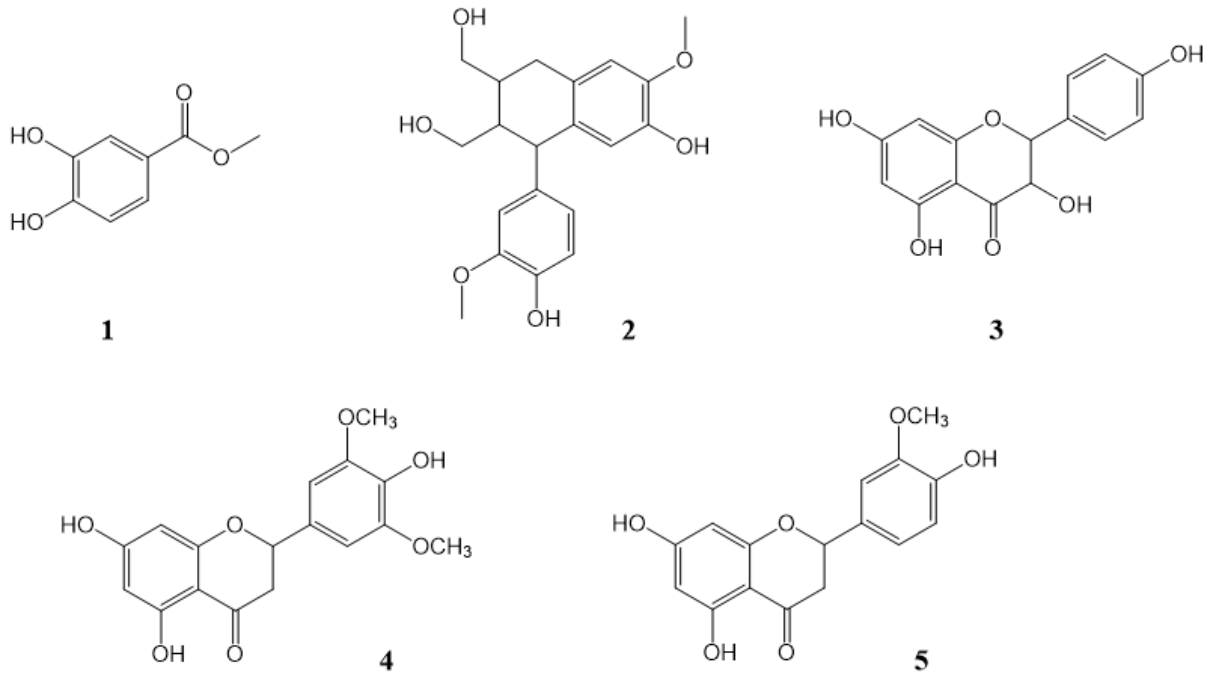

Figure 3.10. Chemical structures of compound **1**, **2, 3**, **4**, **5**.

3.3.4.1 Compound **1**

For compound **1**, the dominant MS/MS fragments (Fig. 3.11) were derived from *m/z* 152.0110 [M-H-•CH_3]$^-$ and *m/z* 108.0211 [M-H-•CH_3-CO_2]$^-$. It was finally assigned as protocatechuic acid methyl ester by comparing with MS and MS/MS spectra of standard compound.

3.3.4.2 Compound **2**

Compound **2** was assigned as isolariciresinol according to the reported MS/MS spectra in literature (Fischer et al., 2012). The matched characteristic fragment ions including ions at *m/z* 344, 329, 323, 159, 255. In addition, the existence of isolariciresinol in methanol açaí was also proved by Chin et.al.

3.3.4.3 Compound **3**

Compound **3** was assigned as dihydrokaempferol by comparing with MS and MS/MS spectra of the standard compound. For a reference, a pure speculation of compound **3**'s major MS/MS fragments was showed in Fig. 3.12. Interestingly enough, an isomer of dihydrokaempferol, maesopsin, had exactly the same MS/MS fragmentation but came out at a different retention time on the same column.

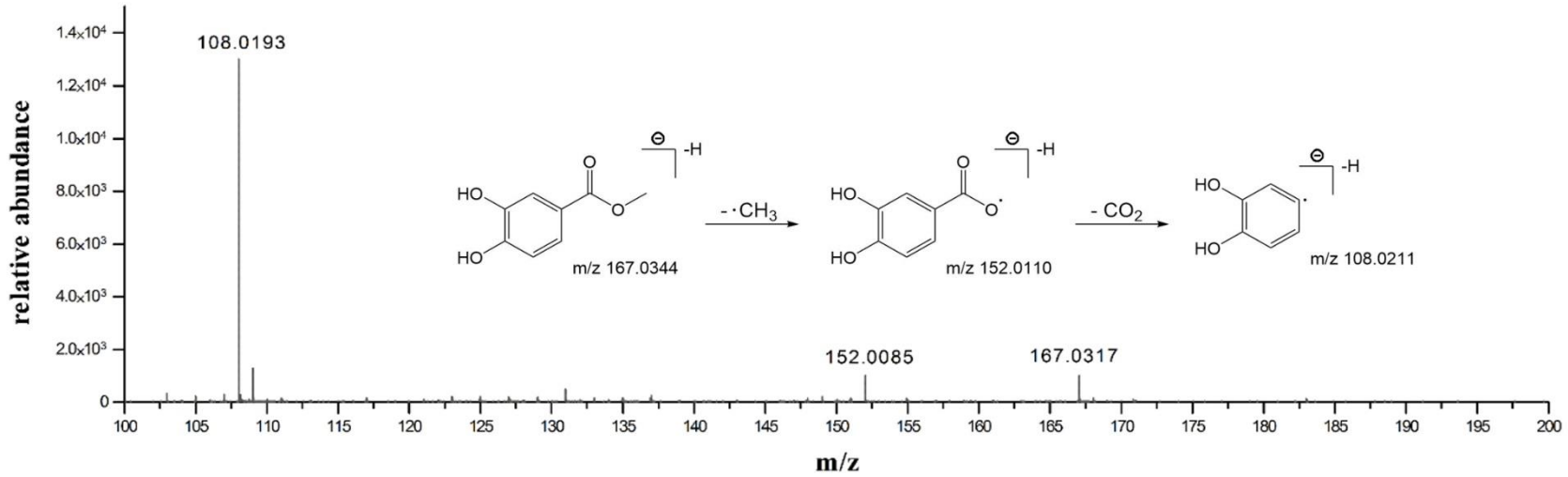

Figure 3.11. Fragmentation pattern and proposed interpretation of compound **1** under 20 eV collision energy.

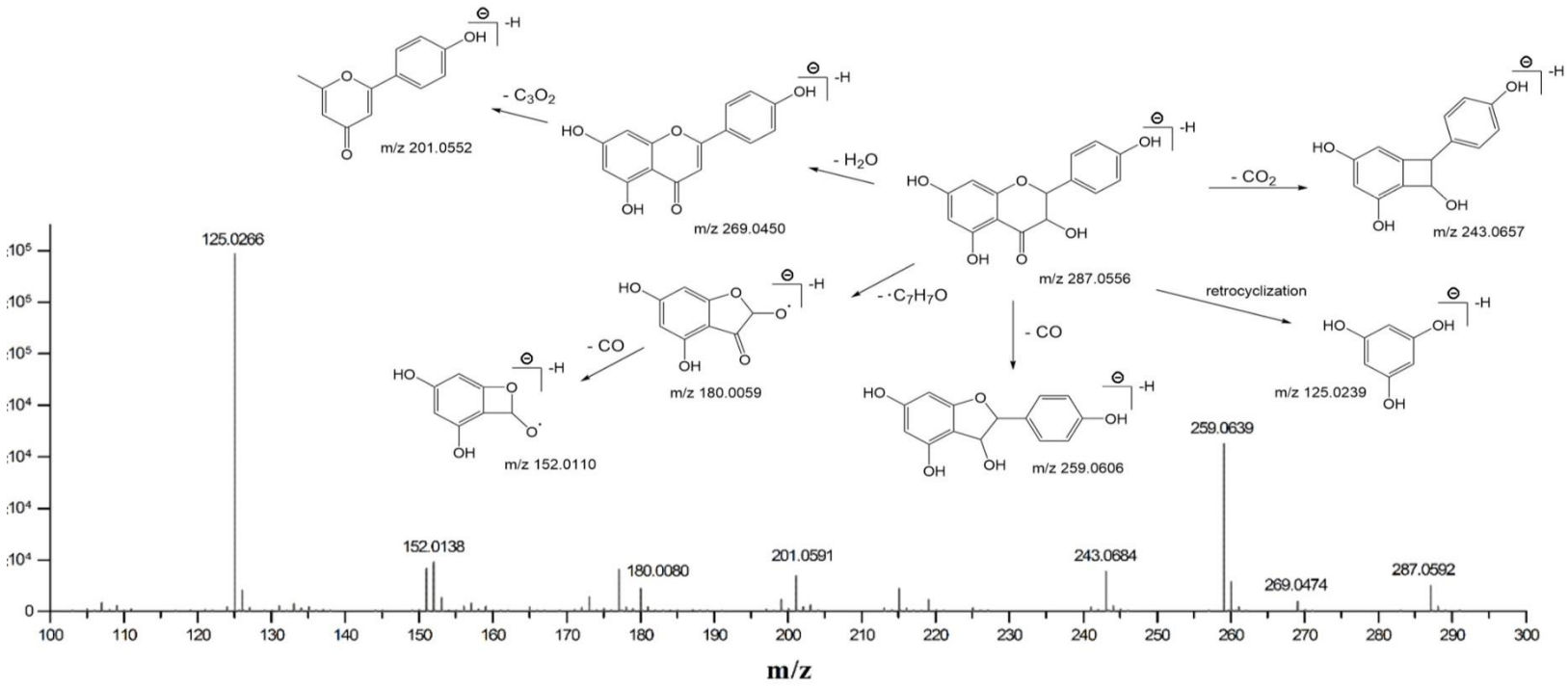

Figure 3.12. Putative fragmentation pattern and proposed interpretation of compound **3** under 20 eV collision energy.

3.3.4.4 Compounds **4** & **5**

Compound **5** was identified as homoeriodictyol by comparing with MS and MS/MS spectra of the standard compound. However, the standard compound of **4** was not commercially available in the market. Therefore, we inferred compound **4**'s chemical structure from its MS/MS fragmentation pattern.

Compound **4** and compound **5** shared very similar MS/MS fragments (Table 3.4, Figures 3.13 and 3.14). A mass shift around *m/z* 30.0061 was observed for peak (2), (4), (7) and (8), while peak (1), (3), (5) and (6) was identified with very close *m/z*. Therefore, their structures should be highly related to each other. According to the literature in interpreting flavonoid's MS/MS spectra (Fabre et al., 2001), a fragmentation interpretation for compound **4** and compound **5** was proposed. In addition, hydroxylation in flavonoids often occur in position 3′ , 4′ and 5′ of ring B (Kumar and Pandey, 2013). Therefore, we inferred that **4** might have one additional methoxy group in position 5′ on homoeriodictyol's B ring. The proposed structure of compound 4 has been found in fruits of Paulownia tomentosa Steud. (Scrophulariaceae) (Smejkal et al., 2007) and the stem of *Dendrobium wardianum* R.Warner (Orchidaceae) (Li et al., 2012), which proves its occurrence in plants.

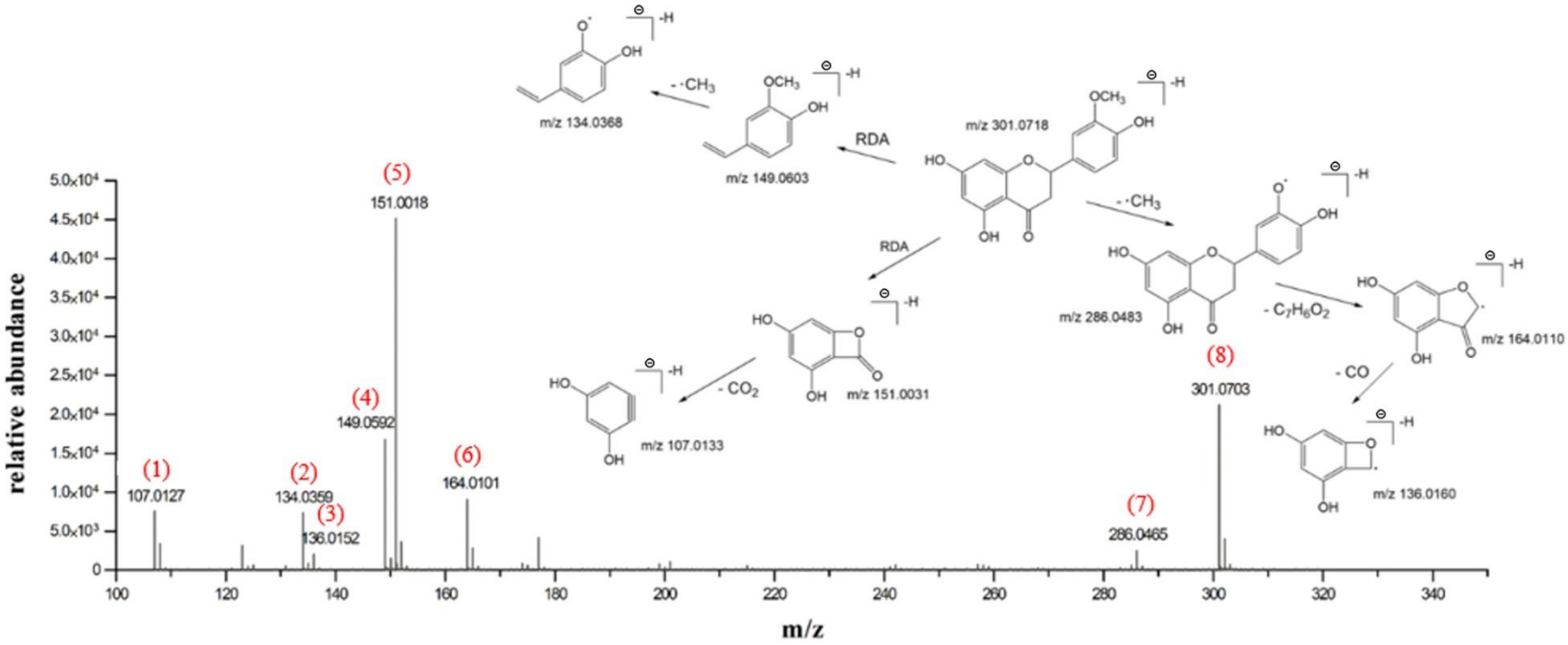

Figure 3.13. Fragmentation pattern and proposed interpretation of compound **5** under 20 eV collision energy.

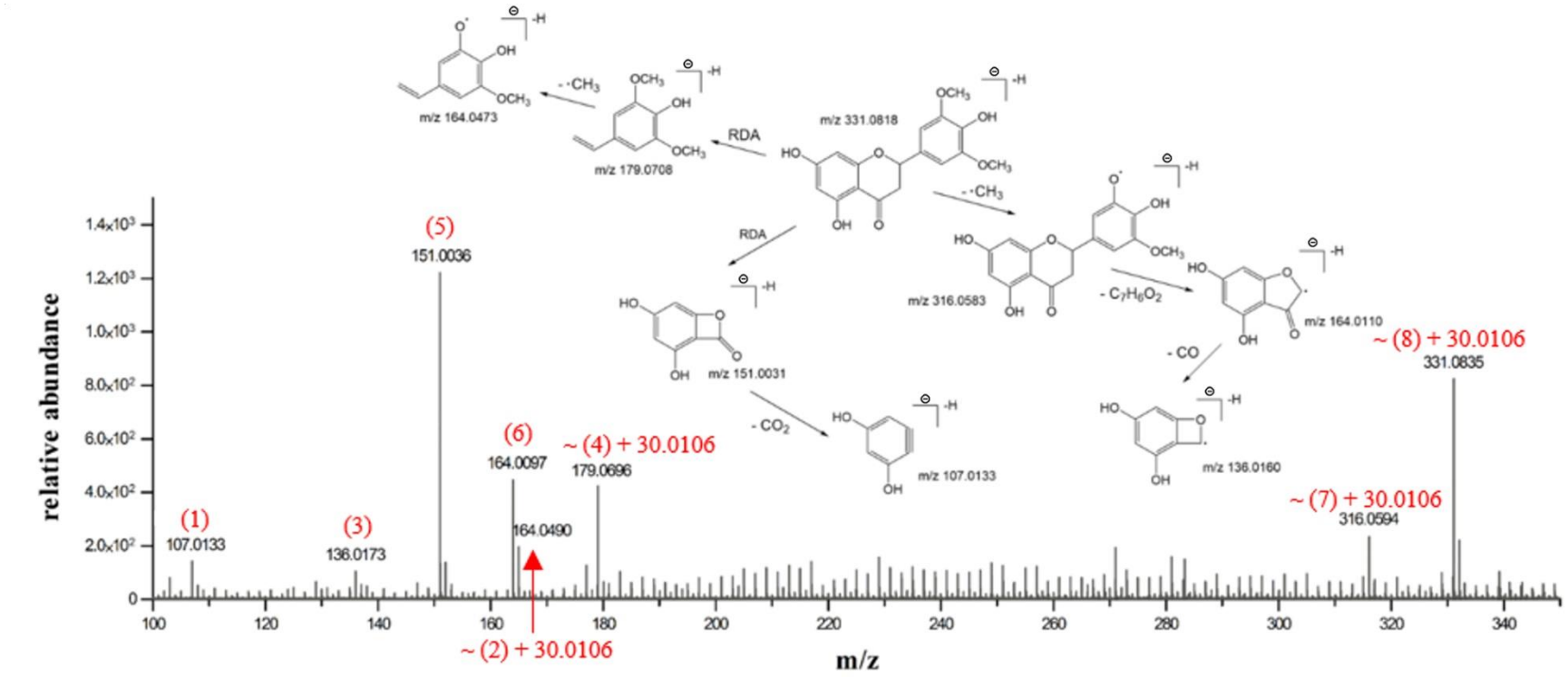

Figure 3.14. Fragmentation pattern and proposed interpretation of compound **4** under 20 eV collision energy.

Table 3.4. Comparison of fragments of compounds **4** & **5** in Figures 3.13 and 3.14 for structure determination.

Fragment number	Compound **4**				Compound **5**			
	Proposed Formula	Accurate mass	Exact mass	Mass error (ppm)	Proposed Formula	Accurate mass	Exact mass	Mass error (ppm)
The identical fragments in compounds **4** & **5**								
(1)	$C_6H_3O_2$	107.0133	107.0133	0.0000	$C_6H_3O_2$	107.0127	107.0133	-5.6068
(3)	$C_7H_4O_3$	136.0173	136.016	9.5576	$C_7H_4O_3$	136.0152	136.016	-5.8817
(5)	$C_7H_3O_4$	151.0036	151.0031	3.3112	$C_7H_3O_4$	151.0018	151.0031	-8.6092
(6)	$C_8H_4O_4$	164.0097	164.011	-7.9264	$C_8H_4O_4$	164.0101	164.011	-5.4875
Fragments that allowed to distinguish compound **4** from **5**								
(2)	$C_9H_8O_3$	164.049	164.0473	10.3628	$C_8H_6O_2$	134.0359	134.0368	-6.7146
(4)	$C_{10}H_{11}O_3$	179.0696	179.0708	-6.7013	$C_9H_9O_2$	149.0592	149.0603	-7.3796
(7)	$C_{16}H_{12}O_7$	316.0594	316.0583	3.4804	$C_{15}H_{10}O_6$	286.0465	286.0483	-6.2927
(8)	$C_{17}H_{15}O_7$	331.0835	331.0818	5.1347	$C_{16}H_{13}O_6$	301.0703	301.0718	-4.9822

Among the five compounds, protocatechuic acid methyl ester, isolariciresinol, and dihydrokaempferol have been previously reported in açaí (Chin et al., 2008). This is the first time the presence of homoeriodictyol was confirmed in açaí. Interestingly, **3** (dihydrokaempferol) and **5** (homoeriodictyol) are known CYP3A4 inhibitors with IC_{50} of 5.79 mM (Budzinski et al., 2000) and < 100 µM (Kimura et al., 2010), respectively. Notably, the two compounds with the highest effective passive permeability, **4** and **5**, were assigned as flavanones. This finding is in agreement with previous data that show that of the flavonoids, flavanones possess the highest passive permeability (Fang et al., 2017).

3.4 UGT-mediated liver metabolism

After 30 minutes incubation, compound **1**, **3** and **5** were transformed to their UGT metabolites at rates of 100%, 50.90% and 99.25%, respectively. As shown in Table 3.5, the UGT-mediated isomeric metabolites were separated by reversed-phase chromatography.

Table 3.5. Calculated mass of parent compounds **1**, **3** and **5** and the corresponding UGT metabolites.

Compound number	Calculated mass $[M - H]^-$	Calculated mass $[M + UGT - H]^-$
1	167.035	343.0671
3	287.0561	463.0882
5	301.0718	477.1038

3.4.1 Tentative identification of metabolites

For all the studied compounds, MS/MS spectra of the metabolic isomers were similar except for the relative abundance of the major fragment ions. This similarity was because the glycoside bond between the glucuronic acid moiety and the parent compound was easily broken during collision-induced dissociation (CID) (van de Wetering et al., 2009). Therefore, the glucuronic acid moiety detached from the parent ion before the backbone fell apart, resulting in a challenge to determine the sites of glucuronidation from LC-MS/MS pattern.

In attempt to propose the tentative structures of the metabolites, two algorithms were used for prediction of site of metabolites. Specifically, predictions are generated through SOMP (http://www.way2drug.com/somp/index.php) and confirmed by XenoSite

(http://swami.wustl.edu/xenosite). The results were showed in Figures 3.15-3.17. The probability of metabolism was calculated based on the following formula:

$$\Delta P = Pt - Pf \quad (3)$$

where Pt is the probability that a labeled atom is the site of metabolism of the appropriate enzyme, while Pf is the probability that the labeled atom is not the site of metabolism.

It was assumed that the EIC peak with the highest ion abundance should correspond to the chemical structure whose site of metabolism had the highest ΔP score.

The assignment of those tentative structures can be confirmed by NMR studies in the future.

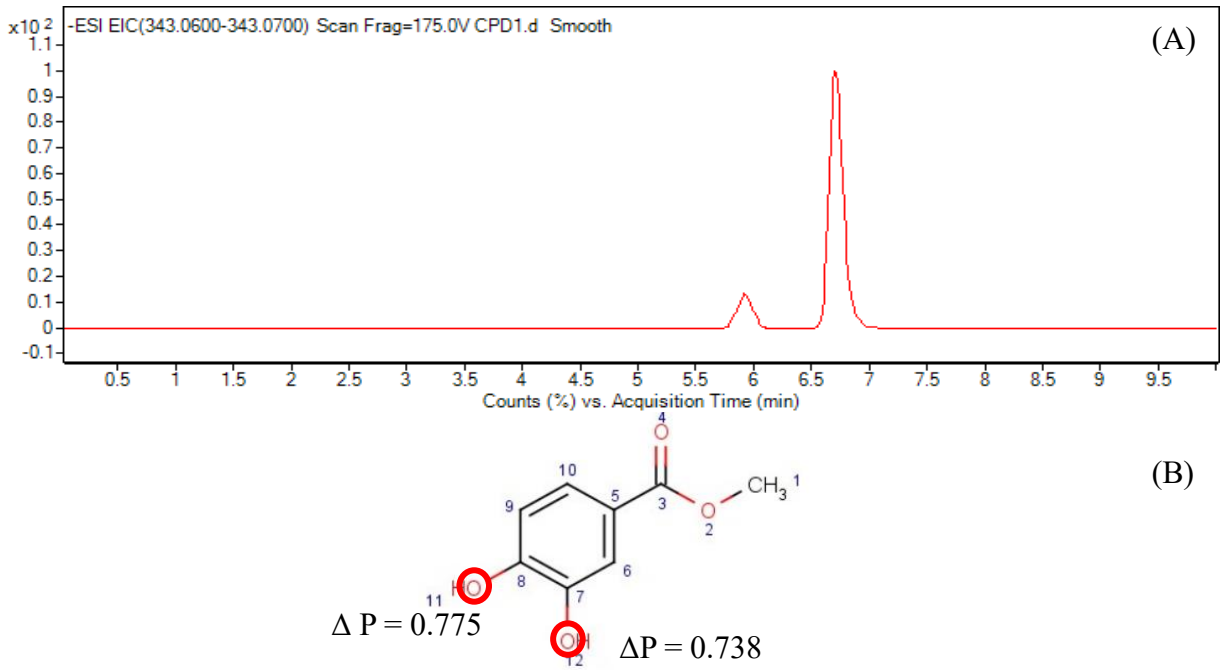

Figure 3.15. Putative UGT-mediated metabolites of compound **1**. (A) EIC of UGT-mediated metabolites of compound **1**, and (B) predicted sites of metabolism.

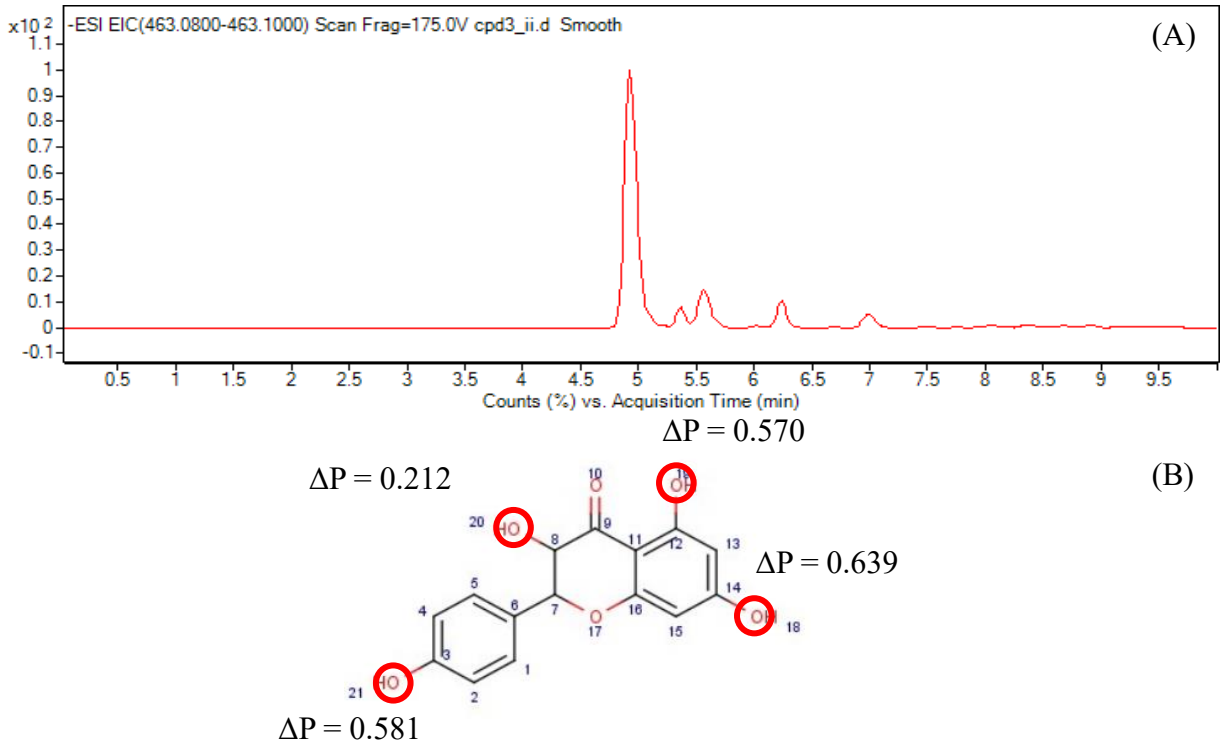

Figure 3.16. Putative UGT-mediated metabolites of compound **3**. (A) EIC of UGT-mediated metabolites of compound **3**, and (B) predicted sites of metabolism.

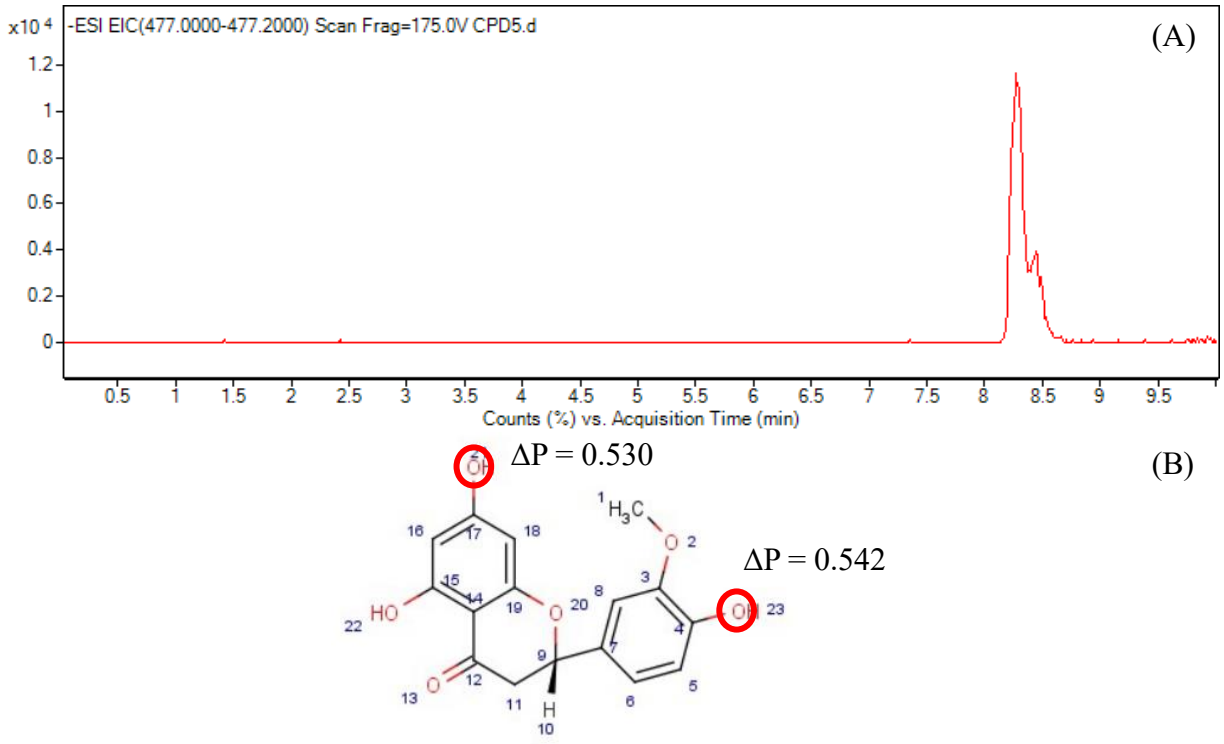

Figure 3.17 Putative UGT-mediated metabolites of compound **5**. (A) EIC of UGT-mediated metabolites of compound **3**, and (B) predicted sites of metabolism.

3.5 CYP-mediated liver metabolism

Based on the liver CYP metabolism assay, compound **3** and **5** experienced little transformation, while the abundance of compound **1** was decreased by 80.15%. In the case of compound **1**, the abundance of a peak at *m/z* 153.0213 was increased compared to the control, which might be generated through deesterification mediated by P450 enzymes. Furthermore, SOMP was used to predict the site of metabolism in compound **1**. As shown in Fig 3.18, atom **1** was the only site with positive ΔP values for P450 isoenzymes (0.733 for CYP3A4, 0.684 for CYP2D6, 0.740 for CYP2C19, 0.601 for CYP2C9, and 0.540 for CYP1A2). Therefore, we assumed that the O-CH3 bond in compound **1** might be cleaved through the metabolism assay, resulting in the formation of protocatechuic acid.

However, we found a relatively small number of cases in which CYP enzymes can be involved in the deesterification of carboxylic acid ester in the literature (Kudo et al., 1999). Considering that protocatechuic acid also existed in the control group, further experiments may need to be performed to prove the assumption.

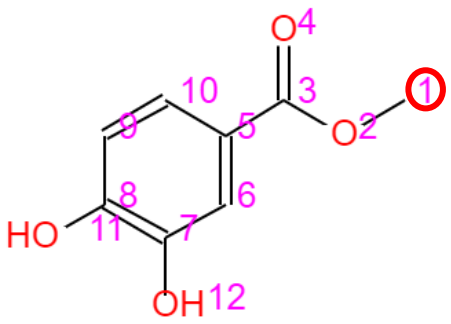

* Most probable CYP metabolism site

Figure 3.18. Numbered structure of compound **1** with the potential site of CYP-mediated metabolism predicted in SOMP.

Compared to UGT-mediated liver metabolism, the transformation rates of all the tested compound were much lower. This founding was consistent with the fact that for polyphenols, phase I metabolism generally plays a less important role compared to phase II metabolic pathways (Gao and Hu, 2010).

3.6 Conclusions

Our study shows that passively diffused compounds in methanol açaí extract have the greatest potential to produce CYP3A4-mediated botanical-drug interactions via both inhibition and induction among the studied plant extracts. The identities of five compounds characterized by high permeability and high abundance in the methanol açaí extract were reported. Generally, this strategy eliminates a significant number of plant constituents, leaving a smaller data set that allows for efficient management and analysis. This innovative strategy may improve the process of accurately identifying botanical extracts with the greatest potential to undergo absorption and to potentially modulate (i.e. inhibit/induce) CYP enzymes. This approach may limit exaggerated results that are often observed in *in vitro* drug metabolism studies.

Besides incorporating PAMPA to improve the *in-vitro* botanical-drug interaction prediction, an *in-vitro* LC-MS-based methodology was established to access human liver metabolites mediated by UGT or CYP enzymes. As a result, a total of 9 metabolites of compounds in methanol açaí extract were separated and annotated successfully. This strategy may be used to further increase the precision of measuring botanical-drug interaction *in vitro*.

This strategy will be performed on formulations of botanical dietary supplements in a subsequent project.

Reference

Abbott, K.L., Chaudhury, C.S., Chandran, A., Vishveshwara, S., Dvorak, Z., Jiskrova, E., Poulikova, K., Vyhlidalova, B., Mani, S., Pondugula, S.R. (2019). Belinostat, at Its Clinically Relevant Concentrations, Inhibits Rifampicin-Induced CYP3A4 and MDR1 Gene Expression. *Mol. Pharmacol. 95*, 324-334.

Atkinson, C., Frankenfeld, C.L., Lampe, J.W. (2005). Gut bacterial metabolism of the soy isoflavone daidzein: exploring the relevance to human health. *Exp. Biol. Med. (Maywood, N.J.) 230*, 155-170.

Avula, B., Smillie, T.J., Wang, Y.H., Zweigenbaum, J., Khan, I.A. (2015). Authentication of true cinnamon (*Cinnamon verum*) utilising direct analysis in real time (DART)-QToF-MS. *Food Addit. Contam., Part A 32*, 1-8.

Awortwe, C., Bouic, P.J., Masimirembwa, C.M., Rosenkranz, B. (2014). Inhibition of major drug metabolizing CYPs by common herbal medicines used by HIV/AIDS patients in Africa--implications for herb-drug interactions. *Drug Metab. Lett. 7*, 83-95.

Awortwe, C., Makiwane, M., Reuter, H., Muller, C., Louw, J., Rosenkranz, B. (2018). Critical evaluation of causality assessment of herb-drug interactions in patients. *Br. J. Clin. Pharmacol. 84*, 679-693.

Balimane, P.V., Han, Y.H., Chong, S. (2006). Current industrial practices of assessing permeability and P-glycoprotein interaction. *AAPS J. 8*, E1-13.

Budzinski, J.W., Foster, B.C., Vandenhoek, S., Arnason, J.T. (2000). An in vitro evaluation of human cytochrome P450 3A4 inhibition by selected commercial herbal extracts and tinctures. *Phytomedicine 7*, 273-282.

Chefson, A., Auclair, K. (2007). CYP3A4 activity in the presence of organic cosolvents, ionic liquids, or water-immiscible organic solvents. *Chembiochem 8*, 1189-1197.

Chin, Y.W., Chai, H.B., Keller, W.J., Kinghorn, A.D. (2008). Lignans and other constituents of the fruits of *Euterpe oleracea* (Acai) with antioxidant and cytoprotective activities. *J. Agric. Food Chem. 56*, 7759-7764.

Clarke, T.C., Black, L.I., Stussman, B.J., Barnes, P.M., Nahin, R.L. (2015). Trends in the use of complementary health approaches among adults: United States, 2002-2012. *Natl. Health Stat. Report*, 1-16.

Cui, B., Zheng, B.L., He, K., Zheng, Q.Y. (2005). Imidazole alkaloids from *Lepidium meyenii* and methods of usage. *U.S. Patent No. 6,878,731*. Washington, DC: U.S. Patent and Trademark Office.

Davis, E.L., Oh, B., Butow, P.N., Mullan, B.A., Clarke, S. (2012). Cancer patient disclosure and patient-doctor communication of complementary and alternative medicine use: a systematic review. *Oncologist 17*, 1475-1481.

de Wildt, S.N., Kearns, G.L., Leeder, J.S., van den Anker, J.N. (1999). Cytochrome P450 3A: ontogeny and drug disposition. *Clin. Pharmacokinet. 37*, 485-505.

Dennison, J.B., Kulanthaivel, P., Barbuch, R.J., Renbarger, J.L., Ehlhardt, W.J., Hall, S.D. (2006). Selective metabolism of vincristine in vitro by CYP3A5. *Drug Metab. Dispos. 34*, 1317-1327.

Dini, A., Migliuolo, G., Rastrelli, L., Saturnino, P., Schettino, O. (1994). Chemical composition of *Lepidium meyenii*. *Food Chem. 49*, 347-349.

Emoto, C., Iwasaki, K. (2006). Enzymatic characteristics of CYP3A5 and CYP3A4: a comparison of in vitro kinetic and drug-drug interaction patterns. *Xenobiotica 36*, 219-233.

Fabre, N., Rustan, I., de Hoffmann, E., Quetin-Leclercq, J. (2001). Determination of flavone, flavonol, and flavanone aglycones by negative ion liquid chromatography electrospray ion trap mass spectrometry. *J. Am. Soc. Mass Spectrom. 12*, 707-715.

Fahim, S.M., Mishuk, A.U., Cheng, N., Hansen, R., Calderon, A.I., Qian, J. (2018). Adverse event reporting patterns of concomitant botanical dietary supplements with CYP3A4 interactive & CYP3A4 non-interactive anticancer drugs in the U.S. Food and Drug Administration Adverse Event Reporting System (FAERS). *Expert opinion on drug safety 18*, 145-152.

Fang, Y., Cao, W., Xia, M., Pan, S., Xu, X. (2017). Study of Structure and Permeability Relationship of Flavonoids in Caco-2 Cells. *Nutrients 9*.

FDA, U. (2003). Guidance for industry: bioavailability and bioequivalence studies for orally administered drug products—general considerations. *Center for Drug Evaluation and Research (CDER), Rockville, MD, USA.*

Fischer, U.A., Jaksch, A.V., Carle, R., Kammerer, D.R. (2012). Determination of lignans in edible and nonedible parts of pomegranate (*Punica granatum* L.) and products derived therefrom, particularly focusing on the quantitation of isolariciresinol using HPLC-DAD-ESI/MSn. *J. Agric. Food Chem. 60*, pp. 283-292

Fisher, M. B., Campanale, K., Ackermann, B. L., VandenBranden, M., & Wrighton, S. A. (2000). In vitro glucuronidation using human liver microsomes and the pore-forming peptide alamethicin. *Drug Metab. Dispos. 28*, 560-566.

Fitzmaurice, C., Allen, C., Barber, R.M., Barregard, L., Bhutta, Z.A., Brenner, H., Dicker, D.J., Chimed-Orchir, O., Dandona, R., Dandona, L., Fleming, T., Forouzanfar, M.H., Hancock, J., Hay, R.J., Hunter-Merrill, R., Huynh, C., Hosgood, H.D., Johnson, C.O., Jonas, J.B., Khubchandani, J., Kumar, G.A., Kutz, M., Lan, Q., Larson, H.J., Liang, X., Lim, S.S., Lopez, A.D., MacIntyre, M.F.,

Marczak, L., Marquez, N., Mokdad, A.H., Pinho, C., Pourmalek, F., Salomon, J.A., Sanabria, J.R., Sandar, L., Sartorius, B., Schwartz, S.M., Shackelford, K.A., Shibuya, K., Stanaway, J., Steiner, C., Sun, J., Takahashi, K., Vollset, S.E., Vos, T., Wagner, J.A., Wang, H., Westerman, R., Zeeb, H., Zoeckler, L., Abd-Allah, F., Ahmed, M.B., Alabed, S., Alam, N.K., Aldhahri, S.F., Alem, G., Alemayohu, M.A., Ali, R., Al-Raddadi, R., Amare, A., Amoako, Y., Artaman, A., Asayesh, H., Atnafu, N., Awasthi, A., Saleem, H.B., Barac, A., Bedi, N., Bensenor, I., Berhane, A., Bernabe, E., Betsu, B., Binagwaho, A., Boneya, D., Campos-Nonato, I., Castaneda-Orjuela, C., Catala-Lopez, F., Chiang, P., Chibueze, C., Chitheer, A., Choi, J.Y., Cowie, B., Damtew, S., das Neves, J., Dey, S., Dharmaratne, S., Dhillon, P., Ding, E., Driscoll, T., Ekwueme, D., Endries, A.Y., Farvid, M., Farzadfar, F., Fernandes, J., Fischer, F., TT, G.H., Gebru, A., Gopalani, S., Hailu, A., Horino, M., Horita, N., Husseini, A., Huybrechts, I., Inoue, M., Islami, F., Jakovljevic, M., James, S., Javanbakht, M., Jee, S.H., Kasaeian, A., Kedir, M.S., Khader, Y.S., Khang, Y.H., Kim, D., Leigh, J., Linn, S., Lunevicius, R., El Razek, H.M.A., Malekzadeh, R., Malta, D.C., Marcenes, W., Markos, D., Melaku, Y.A., Meles, K.G., Mendoza, W., Mengiste, D.T., Meretoja, T.J., Miller, T.R., Mohammad, K.A., Mohammadi, A., Mohammed, S., Moradi-Lakeh, M., Nagel, G., Nand, D., Le Nguyen, Q., Nolte, S., Ogbo, F.A., Oladimeji, K.E., Oren, E., Pa, M., Park, E.K., Pereira, D.M., Plass, D., Qorbani, M., Radfar, A., Rafay, A., Rahman, M., Rana, S.M., Soreide, K., Satpathy, M., Sawhney, M., Sepanlou, S.G., Shaikh, M.A., She, J., Shiue, I., Shore, H.R., Shrime, M.G., So, S., Soneji, S., Stathopoulou, V., Stroumpoulis, K., Sufiyan, M.B., Sykes, B.L., Tabares-Seisdedos, R., Tadese, F., Tedla, B.A., Tessema, G.A., Thakur, J.S., Tran, B.X., Ukwaja, K.N., Uzochukwu, B.S.C., Vlassov, V.V., Weiderpass, E., Wubshet Terefe, M., Yebyo, H.G., Yimam, H.H., Yonemoto, N., Younis, M.Z., Yu, C., Zaidi, Z., Zaki, M.E.S., Zenebe, Z.M., Murray, C.J.L., Naghavi, M. (2017). Global, Regional, and National Cancer Incidence, Mortality, Years of Life

Lost, Years Lived With Disability, and Disability-Adjusted Life-years for 32 Cancer Groups, 1990 to 2015: A Systematic Analysis for the Global Burden of Disease Study. *JAMA Oncol. 3,* 524-548.

Gao, S., Hu, M. (2010). Bioavailability challenges associated with development of anti-cancer phenolics. *Mini-Rev. Med. Chem. 10,* 550-567.

Gu, Q., David, F., Lynen, F., Rumpel, K., Dugardeyn, J., Van Der Straeten, D., Xu, G., Sandra, P. (2011). Evaluation of automated sample preparation, retention time locked gas chromatography-mass spectrometry and data analysis methods for the metabolomic study of *Arabidopsis* species. *J. Chromatogr. A 1218*, 3247-3254.

Gurley, B.J., Yates, C.R., Markowitz, J.S. (2018). "...Not Intended to Diagnose, Treat, Cure or Prevent Any Disease." 25 Years of Botanical Dietary Supplement Research and the Lessons Learned. *Clin. Pharmacol. Ther. 104*, 470-483.

Hermann, M. (1997). Andean roots and tubers: ahipa, arracacha, maca and yacon (Vol. 21). International Potato Center.

Hu, J., Zhao, J., Khan, S.I., Liu, Q., Liu, Y., Ali, Z., Li, X.C., Zhang, S.H., Cai, X., Huang, H.Y., Wang, W., Khan, I.A. (2014). Antioxidant neolignan and phenolic glucosides from the fruit of *Euterpe oleracea*. *Fitoterapia 99*, 178-183.

Huang, K., Huang, L., van Breemen, R.B. (2015). Detection of reactive metabolites using isotope-labeled glutathione trapping and simultaneous neutral loss and precursor ion scanning with ultra-high-pressure liquid chromatography triple quadruple mass spectrometry. *Anal. Chem. 87*, 3646-3654.

Izzo, A.A. (2012). Interactions between herbs and conventional drugs: overview of the clinical data. *Med. Princ. Pract. 21*, 404-428.

Jensen, G.S., Wu, X., Patterson, K.M., Barnes, J., Carter, S.G., Scherwitz, L., Beaman, R., Endres, J.R., Schauss, A.G. (2008). In vitro and in vivo antioxidant and anti-inflammatory capacities of an antioxidant-rich fruit and berry juice blend. Results of a pilot and randomized, double-blinded, placebo-controlled, crossover study. *J. Agric. Food Chem. 56*, 8326-8333.

Kidd, P.M. (2009). Bioavailability and activity of phytosome complexes from botanical polyphenols: the silymarin, curcumin, green tea, and grape seed extracts. *Altern. Med. Rev. 14*, 226-246.

Kimura, Y., Ito, H., Ohnishi, R., Hatano, T. (2010). Inhibitory effects of polyphenols on human cytochrome P450 3A4 and 2C9 activity. *Food Chem. Toxicol. 48*, 429-435.

Kudo, S., Okumura, H., Miyamoto, G., Ishizaki, T. (1999). Cytochrome P-450 isoforms involved in carboxylic acid ester cleavage of Hantzsch pyridine ester of pranidipine. *Drug Metab. Dispos. 27*, 303-308.

Kumar, S., Pandey, A.K. (2013). Chemistry and biological activities of flavonoids: an overview. *Sci. World J. 2013*.

Lampe, J.W., Chang, J.L. (2007). Interindividual differences in phytochemical metabolism and disposition. *Semin. Cancer Biol. 17*, 347-353.

Lazaro, E., Lowe, P.J., Briand, X., Faller, B. (2008). New approach to measure protein binding based on a parallel artificial membrane assay and human serum albumin. *J. Med. Chem. 51*, 2009-2017.

Lea, T. (2015). Caco-2 cell line. In 'The impact of food bioactives on health: and models'.(Eds K Verhoeckx, P Cotter, I López-Expósito, C Kleiveland, T Lea, A Mackie, T Requena, D Swiatecka, H Wichers) pp. 103–113.

Li, C., Hansen, R.A., Chou, C., Calderon, A.I., Qian, J. (2018). Trends in botanical dietary supplement use among US adults by cancer status: The National Health and Nutrition Examination Survey, 1999 to 2014. *Cancer 124*, 1207-1215.

Li, J., Zhao, M., He, P., Hidalgo, M., Baker, S.D. (2007). Differential metabolism of gefitinib and erlotinib by human cytochrome P450 enzymes. *Clin. Cancer Res. 13*, 3731-3737.

Loypimai, P., Moongngarm, A., Chottanom, P. (2016). Thermal and pH degradation kinetics of anthocyanins in natural food colorant prepared from black rice bran. *J. Food Sci. Technol. 53*, 461-470.

Lynch, T., Price, A. (2007). The effect of cytochrome P450 metabolism on drug response, interactions, and adverse effects. *Am. Fam. Physician 76*, 391-396.

Markowitz, J.S., von Moltke, L.L., Donovan, J.L. (2008). Predicting interactions between conventional medications and botanical products on the basis of in vitro investigations. *Mol. Nutr. Food Res. 52*, 747-754.

Markowitz, J.S., Zhu, H.J. (2012). Limitations of in vitro assessments of the drug interaction potential of botanical supplements. *Planta Med. 78*, 1421-1427.

Matsson, P., Bergstrom, C.A., Nagahara, N., Tavelin, S., Norinder, U., Artursson, P. (2005). Exploring the role of different drug transport routes in permeability screening. *J. Med. Chem. 48*, 604-613.

Mertens-Talcott, S.U., Rios, J., Jilma-Stohlawetz, P., Pacheco-Palencia, L.A., Meibohm, B., Talcott, S.T., Derendorf, H. (2008). Pharmacokinetics of anthocyanins and antioxidant effects after the consumption of anthocyanin-rich acai juice and pulp (*Euterpe oleracea* Mart.) in human healthy volunteers. *J. Agric. Food Chem. 56*, 7796-7802.

Mudie, D.M., Murray, K., Hoad, C.L., Pritchard, S.E., Garnett, M.C., Amidon, G.L., Gowland, P.A., Spiller, R.C., Amidon, G.E., Marciani, L. (2014). Quantification of gastrointestinal liquid volumes and distribution following a 240 mL dose of water in the fasted state. *Mol. Pharmaceutics 11*, 3039-3047.

Musharraf, S.G., Mazhar, S., Choudhary, M.I., Rizi, N., Atta ur, R. (2015). Plasma metabolite profiling and chemometric analyses of lung cancer along with three controls through gas chromatography-mass spectrometry. *Sci. Rep. 5*, 8607.

Nachshon-Kedmi, M., Yannai, S., Fares, F.A. (2004). Induction of apoptosis in human prostate cancer cell line, PC3, by 3,3'-diindolylmethane through the mitochondrial pathway. *Br. J. Cancer 91*, 1358-1363.

Nebot, N., Crettol, S., d'Esposito, F., Tattam, B., Hibbs, D.E., Murray, M. (2010). Participation of CYP2C8 and CYP3A4 in the N-demethylation of imatinib in human hepatic microsomes. *Br. J. Pharmacol. 161*, 1059-1069.

NIH. (2018). URL https://dsld.nlm.nih.gov/dsld/index.jsp Accessed 08/30/2017.

Ortiz de Montellano, P.R. (2013). Cytochrome P450-activated prodrugs. *Future Med. Chem. 5*, 213-228.

Petit, C., Bujard, A., Skalicka-Wozniak, K., Cretton, S., Houriet, J., Christen, P., Carrupt, P.A., Wolfender, J.L. (2016). Prediction of the passive intestinal absorption of medicinal plant extract constituents with the parallel artificial membrane permeability assay (PAMPA). *Planta Med. 82*, 424-431.

Pondugula, S.R., Ferniany, G., Ashraf, F., Abbott, K.L., Smith, B.F., Coleman, E.S., Mansour, M., Bird, R.C., Smith, A.N., Karthikeyan, C., Trivedi, P., Tiwari, A.K. (2015a). Stearidonic acid, a

plant-based dietary fatty acid, enhances the chemosensitivity of canine lymphoid tumor cells. *Biochem. Biophys. Res. Commun. 460*, 1002-1007.

Pondugula, S.R., Flannery, P.C., Abbott, K.L., Coleman, E.S., Mani, S., Samuel, T., Xie, W. (2015b). Diindolylmethane, a naturally occurring compound, induces CYP3A4 and MDR1 gene expression by activating human PXR. *Toxicol. Lett. 232*, 580-589.

Quiroz, C., Aliaga, R., Hermann, M., Hellers, J. (1997). Andean roots and tubers: ahipa, arracacha, maca and yacon. *International Plant Genetic Resources Institute, Rome, Italy*.

Rocha, A.P., Carvalho, L.C., Sousa, M.A., Madeira, S.V., Sousa, P.J., Tano, T., Schini-Kerth, V.B., Resende, A.C., Soares de Moura, R. (2007). Endothelium-dependent vasodilator effect of *Euterpe oleracea* Mart. (Acai) extracts in mesenteric vascular bed of the rat. *Vasc. Pharmacol. 46*, 97-104.

Roy, J.N., Lajoie, J., Zijenah, L.S., Barama, A., Poirier, C., Ward, B.J., Roger, M. (2005). CYP3A5 genetic polymorphisms in different ethnic populations. *Drug Metab. Dispos. 33*, 884-887.

Sadowska-Krepa, E., Klapcinska, B., Podgorski, T., Szade, B., Tyl, K., Hadzik, A. (2015). Effects of supplementation with acai (*Euterpe oleracea* Mart.) berry-based juice blend on the blood antioxidant defence capacity and lipid profile in junior hurdlers. A pilot study. *Biol. Sport 32*, 161-168.

Sandoval, M., Okuhama, N.N., Angeles, F.M., Melchor, V.V., Condezo, L.A., Lao, J., Miller, M.J. (2002). Antioxidant activity of the cruciferous vegetable Maca (*Lepidium meyenii*). *Food Chem. 79*, 207-213.

Santos, A., Zanetta, S., Cresteil, T., Deroussent, A., Pein, F., Raymond, E., Vernillet, L., Risse, M.L., Boige, V., Gouyette, A., Vassal, G. (2000). Metabolism of irinotecan (CPT-11) by CYP3A4 and CYP3A5 in humans. *Clin. Cancer Res. 6*, 2012-2020.

Schauss, A.G., Wu, X., Prior, R.L., Ou, B., Huang, D., Owens, J., Agarwal, A., Jensen, G.S., Hart, A.N., Shanbrom, E. (2006). Antioxidant capacity and other bioactivities of the freeze-dried Amazonian palm berry, *Euterpe oleraceae* Mart. (acai). *J. Agric. Food Chem. 54*, 8604-8610.

Schiller, C., Frohlich, C.P., Giessmann, T., Siegmund, W., Monnikes, H., Hosten, N., Weitschies, W. (2005). Intestinal fluid volumes and transit of dosage forms as assessed by magnetic resonance imaging. *Aliment. Pharmacol. Ther. 22*, 971-979.

Scripture, C.D., Figg, W.D. (2006). Drug interactions in cancer therapy. *Nat. Rev. Cancer 6*, 546-558.

Shipkowski, K.A., Betz, J.M., Birnbaum, L.S., Bucher, J.R., Coates, P.M., Hopp, D.C., MacKay, D., Oketch-Rabah, H., Walker, N.J., Welch, C., Rider, C.V. (2018). Naturally complex: Perspectives and challenges associated with Botanical Dietary Supplement Safety assessment. Food Chem. *Toxicol. 118*, 963-971.

Shou, M., Martinet, M., Korzekwa, K.R., Krausz, K.W., Gonzalez, F.J., Gelboin, H.V. (1998). Role of human cytochrome P450 3A4 and 3A5 in the metabolism of taxotere and its derivatives: enzyme specificity, interindividual distribution and metabolic contribution in human liver. *Pharmacogenetics 8*, 391-401.

Sprouse, A.A., van Breemen, R.B. (2016). Pharmacokinetic Interactions between Drugs and Botanical Dietary Supplements. *Drug Metab. Dispos. 44*, 162-171.

Sterling, H.J., Batchelor, J.D., Wemmer, D.E., Williams, E.R. (2010). Effects of buffer loading for electrospray ionization mass spectrometry of a noncovalent protein complex that requires high concentrations of essential salts. *J. Am. Soc. Mass Spectrom. 21*, 1045-1049.

Tascilar, M., de Jong, F.A., Verweij, J., Mathijssen, R.H. (2006). Complementary and alternative medicine during cancer treatment: beyond innocence. *Oncologist 11*, 732-741.

Tornio, A., Filppula, A.M., Kailari, O., Neuvonen, M., Nyronen, T.H., Tapaninen, T., Neuvonen, P.J., Niemi, M., Backman, J.T. (2014). Glucuronidation converts clopidogrel to a strong time-dependent inhibitor of CYP2C8: a phase II metabolite as a perpetrator of drug-drug interactions. *Clin. Pharmacol. Ther. 96*, 498-507.

Vaclavik, L., Lacina, O., Hajslova, J., Zweigenbaum, J. (2011). The use of high performance liquid chromatography-quadrupole time-of-flight mass spectrometry coupled to advanced data mining and chemometric tools for discrimination and classification of red wines according to their variety. *Anal. Chim. Acta 685,* 45-51.

van de Wetering, K., Feddema, W., Helms, J.B., Brouwers, J.F., Borst, P. (2009). Targeted metabolomics identifies glucuronides of dietary phytoestrogens as a major class of MRP3 substrates in vivo. *Gastroenterology 137*, 1725-1735.

Vizcaino, M.I., Crawford, J.M. (2016). Secondary Metabolic Pathway-Targeted Metabolomics. *Methods Mol. Biol. (Clifton, N.J.) 1401*, 175-195.

Walsky, R.L., Obach, R.S., Hyland, R., Kang, P., Zhou, S., West, M., Geoghegan, K.F., Helal, C.J., Walker, G.S., Goosen, T.C., Zientek, M.A. (2012). Selective mechanism-based inactivation of CYP3A4 by CYP3cide (PF-04981517) and its utility as an in vitro tool for delineating the relative roles of CYP3A4 versus CYP3A5 in the metabolism of drugs. *Drug Metab. Dispos. 40,* 1686-1697.

Williams, J.A., Cook, J., Hurst, S.I. (2003). A significant drug-metabolizing role for CYP3A5? *Drug Metab. Dispos. 31*, 1526-1530.

Xia, C., Chen, J., Deng, J., Zhu, Y., Li, W., Jie, B., Chen, T. (2018). Novel macamides from maca (*Lepidium meyenii* Walpers) root and their cytotoxicity. *Phytochem. Lett. 25*, 65-69.

Yamaguchi, K.K., Pereira, L.F., Lamarao, C.V., Lima, E.S., da Veiga-Junior, V.F. (2015). Amazon acai: chemistry and biological activities: a review. *Food Chem. 179*, 137-151.

Yu, M., Qin, X., Peng, X., Wang, X., Tian, X., Li, Z., Qiu, M. (2017). Macathiohydantoins B–K, novel thiohydantoin derivatives from *Lepidium meyenii*. *Tetrahedron 73*, 4392-4397.

Yuan, R., Madani, S., Wei, X.X., Reynolds, K., Huang, S.M. (2002). Evaluation of cytochrome P450 probe substrates commonly used by the pharmaceutical industry to study in vitro drug interactions. *Drug Metab. Dispos. 30*, 1311-1319.

Zaltzman, A.S., Glick, L.A., Zaltzman, J.S., Nash, M., Huang, M., Prasad, G.V. (2016). The role of CYP3A5 polymorphism and dose adjustments following conversion of twice-daily to once-daily tacrolimus in renal transplant recipients. *Transplant. Res. 5*, 2.

Zareba, G. (2009). Phytotherapy for pain relief. *Drugs Today 45*, 445-467.

Zheng, B.L., He, K., Kim, C.H., Rogers, L., Shao, Y., Huang, Z.Y., Lu, Y., Yan, S.J., Qien, L.C., Zheng, Q.Y. (2000). Effect of a lipidic extract from *lepidium meyenii* on sexual behavior in mice and rats. Urology 55, 598-602.

Zhuo, X., Zheng, N., Felix, C.A., Blair, I.A. (2004). Kinetics and regulation of cytochrome P450-mediated etoposide metabolism. Drug Metab. Dispos. 32, 993-1000.